

Spectroscopic Study on the Photocycle of the LOV2
Domain from *Chlamidomonas reinhardtii* and
Its Interaction with LOV1



DISSERTATION
zur Erlangung des Doktorgrades
der Naturwissenschaften (Dr. rer. nat.) der Fakultät IV
-Chemie und Pharmazie-
der Universität Regensburg

vorgelegt von
Huimin Guo
aus China

Regensburg 2005

Promotionsgesuch eingereicht am : 4. July. 2005

Diese Arbeit wurde angeleitet von : Prof. Dr. B. Dick

Prüfungsausschuss : Prof. Dr. H. Krienke

Prof. Dr. B. Dick

Prof. Dr. P. Hegemann

Prof. Dr. J. Daub

Table of contents

1	Introduction	1
1.1	About Phototropin.....	2
1.2	Goals	5
2	Materials and Experimental Methods	7
2.1	Phototropin from <i>Chlamidomonas reinhardtii</i>	7
2.1.1	Sequence.....	7
2.1.2	Crystal Structure of LOV Domains.....	8
2.2	Protein Preparation	11
2.2.1	Wild-type.....	11
2.2.2	Mutants	12
2.2.3	Purification	12
2.2.4	Gel Chromatography	12
2.3	Experimental Methods.....	13
2.3.1	Flash Photolysis.....	13
2.3.2	UV/Vis Spectra.....	15

2.3.3 Slow and fast Bleaching Kinetics	17
3 Results	18
3.1 Dark Form.....	18
3.1.1 UV-Vis Absorption Spectra	18
3.2 Triplet state	21
3.2.1 Decay of the triplet excited State	21
3.3 Decay of the Adduct	28
3.3.1 Decay Kinetics	28
3.3.2 pH Effect	32
3.3.3 Influence of NaCl Concentration	38
3.3.4 Activation Energy of Bond Cleavage in the Adduct.....	41
3.3.5 H/D Isotope Effect on the Thermal Backreaction.....	44
3.3.6 Photoreaction of the Mutant LOV1-C57G.....	45
3.3.7 Photochemical Back-reaction.....	47
4 The Photocycle of LOV2	53
5 Comparison of Models for the Photocycle	56
5.1 Global fit procedure	56
5.2 Models.....	61
5.3 Analysis of data for LOV1.....	65

5.4 Analysis of data for LOV2.....	69
5.5 Analysis of data for LOV1+2	70
6 Mechanism of the formation of the adduct	73
6.1 Possible photoreaction scheme of the adduct formation	73
6.1.1 Ionic Model	74
6.1.2 Nucleophilic Model.....	75
6.1.3 Radical-pair Model.....	77
7 Summary	79
8 Appendix	83
9 References	85
Acknowledgement	94

1 Introduction

Light is one of the most important abiotic factors influencing plant growth and development. A wide range of phenomena in the life cycle of plants such as circadian timing, seed germination, pigment biosynthesis, regulation of gene expression, floral induction, and phototropism are all responses to ambient light levels in the growth environment of the plant [1-3]. Control of these responses in higher plants is located primarily within specific wavelength bands in the red or ultraviolet (UV)-visible (VIS) spectral regions, which are perceived by different photoreceptors [4]. Several different photoreceptor families are known to mediate the effects of the light on plant development [5]: the bilin-binding phytochromes mediate responses to red and far-red light [6], whereas cryptochromes [7], BLUF (blue light sensing using FAD) domain containing with FAD (flavin adenine dinucleotide) as chromophore [8, 9], and phototropins [10] with FMN (flavin mononucleotide) as the chromophoric molecule mediate responses to blue light. There are several other classes of photosensory receptors responsive to blue light [11], such as photoactive yellow proteins (PYP) in photosynthetic bacteria [12], retinal proteins homologous to archaeal rhodopsins [13], and photoactivated adenylyl cyclase (PAC) as *Euglena*'s blue light receptor [14], which have been discovered in the last decade. This thesis presents our studies of the phototropin from *Chlamydomonas reinhardtii*.

1.1 About Phototropin

Although it was known for a long time that UV and blue light regulate a wide range of responses in plants, including phototropism (plant growth towards the light source) [15], chloroplast migration [16], and stomatal opening [17], the photoreceptors for these light responses have been identified only in recent years. Phototropins, recently renamed Phot proteins [2,3], represent a class of blue-light sensitive receptor kinases, which belong to the PAS domain superfamily originally characterized in PER, ARNT, SIM proteins. There are at least two kinds of types in this family, Phot1 and Phot2. These have formerly been named nph1 for nonphototropic hypocotyls-1 and npl1 for nph1-like, respectively [18]. Characteristic for phototropins is that each Phot contains two flavin mononucleotide (FMN)-binding LOV (light-, oxygen-, voltage-sensitive) domains at its N-terminus and a serine/threonine protein kinase domain at its C-terminus [19]. Generally, these two LOV domains are named LOV1 and LOV2. Each consists of approximately 100 amino acids, and differences in their sequences define them as either LOV1 or LOV2. They are separated by an intervening sequence of variable length. Upon blue light illumination of the protein the serine/threonine kinase is activated and multiple auto-phosphorylation is observed [20].

All LOV domains demonstrate qualitatively identical and fully reversible photocycles, governed by the same general reaction mechanism [21]. Thus they provide an excellent system for investigation of the photochemical properties of the blue light receptor phototropin. In recent years, phototropin has been successfully expressed in *Escherichia. Coli*, isolated, and purified. Subsequent spectroscopic experiments and biochemical analysis provided much insight into the photochemical properties and reaction mechanism underlying blue light perception by phototropin.

Introduction

When LOV domains are illuminated with blue light, they undergo a spectral change, characterized by a loss of absorption in the blue region of the spectrum combined with the appearance of a new absorption band with peak near 390 nm (see Figure 3.6). The absorbance changes are not those of the typical reduction reactions of FMN but resemble those observed for the formation of an adduct between a cysteine residue and the C(4a) carbon of the FMN chromophore previously observed for the mercuric ion reductase of the ACAA mutant [22]. In phototropin, the formation of this photoproduct occurs within a few microseconds following the absorption of the blue light photon [23]. When the illumination ceases, i.e. under dark condition, this adduct reverts to the dark form of the LOV domains. In addition, the mutation of a highly conserved cysteine in LOV domains to alanine or serine completely abolishes the photochemical reactivity. Therefore, the cysteinyl-adduct formation probably represents the primary photoreaction underlying light detection by the phototropins [24].

In recent years this hypothesis has been verified by NMR spectroscopy studies on LOV2 domain from *Avena sativa* [25], by FTIR spectroscopy studies on LOV2 domain from Oat [26], and by X-ray crystallography of a LOV2 domain from *Adiantum capillus-veneris* [27] and a LOV1 domain from *Chlamydomonas reinhardtii* [28]. The position of the reactive cysteine is C450 in *Avena sativa* LOV2 domain, C966 in *Adiantum capillus-veneris* LOV2 domain, and C57 and C250 in *Chlamydomonas reinhardtii* LOV1 and LOV2 domains, respectively [29]. The photoproduct (LOV-390) produced by irradiation with blue light thermally reverts to the ground state (LOV-447) on the minute time scale in the dark, with a pH and salt concentration dependent time constant [30].

Many details of the mechanism of this photocycle of various LOV domains from different organisms are still unknown, though some progress has been made. At the moment the commonly accepted sequence of photophysical and photochemical reactions in the LOV

Introduction

domains involve ISC (intersystem crossing) from the excited singlet state of FMN to the triplet excited state ($S_1 \rightarrow T_1$), characterized by a broad absorption band at about 660 nm and peak at 715 nm. Hence this species has been named LOV-715. The subsequent mechanistic steps of photoproduct formation are, however, still controversially discussed. It has been suggested that H^+ -transfer from the thiol group to the N(5)-position of the isoalloxazine ring is the rate-limiting step of the adduct formation [21]. But studies on a LOV1 mutant, in which the reactive cysteine was displaced by methionine, made it more likely that an electron transfer from the protein sulfur atom to FMN is the primary and rate-limiting step [31, 32]. This step would be followed by proton transfer to FMN resulting in a pair of neutral radicals which would eventually combine to form the adduct. This model is consistent with the results of time-resolved EPR measurements on several LOV domains, which lead to the conclusion that the radical pair mechanism is dominating the pathway from the triplet state to the adduct under most reaction conditions [33, 34]. Low-temperature studies with time-resolved EPR and UV/Vis spectroscopy on a LOV domain revealed that the light-induced flavin adduct can be formed even at temperature lower than 80K [34], which suggest that the process takes place without much structural rearrangement in the protein. This discovery is in remarkable contrast to other light sensor proteins, like rhodopsins, phytochromes, and PYP (photoactive yellow protein) [35]. In these photoreceptor systems photoisomerization occurs on a femtosecond or picosecond time scale, whereas the intermediates activating transducer appear in milliseconds or seconds, which might indicate that the phototropic response is the result of a complex signal transduction system.

So far the details of the interaction between the LOV domains and the kinase in phototropins is still not known. It was found by NMR spectroscopy that the short α -helix connecting LOV2 with the kinase associates with the LOV2 core under dark conditions but not in the light [36].

Fluorescence measurements on LOV domains from several organisms displayed that the decay kinetics of LOV-390 in peptides containing both LOV domains is obviously slower than that of the isolated domains [37]. Through similar investigations on Phot2 from the fern *Adiantum capillus-veneris*, it was suggested that LOV1 reduces the lifetime of the domain pair LOV1+2 signal in order to limit the physiological response at strong light level [38]. Moreover, the data obtained from the tandem LOV domain fusion proteins closely resemble those from the full-length proteins. This certainly indicates a relevant interaction between the two LOV domains. But how the photoreactions of LOV1 or LOV2 influence the interaction is not clear. In this dissertation, we also pay much attention to this problem and try to understand the interaction between two LOV domains through the studies on the individual and double domains.

1.2 Goals

Three blue-light photoreceptor families are presently known, namely phototropins, BLUF-domains, and cryptochromes, of these, only the photoproduct of the phototropins has been identified so far, which is the thioadduct of the FMN and the cysteine in the LOV domains. For other domains spectra of the light activated domains have been reported, but their chemical structure is completely unknown.

But also in the case of LOV domains, although the thioadduct is generally accepted as the primary photoproduct, many details of the mechanism of adduct formation and the subsequent steps of activation and signal transduction have to be unraveled. In this thesis, we present the results of our studies on the two LOV domains from Phot1 of *Chlamydomonas reinhardtii*. The photocycle of LOV1 has been the topic of a previous thesis [39]. In this thesis, the triplet intermediate was characterized, and a decelerating effect of acidic conditions on the thermal

Introduction

backreaction was observed in the pH range from 3.5 to 8.0, which was enhanced by high salt concentration.

In the present thesis, the photocycle of LOV2 will be characterized in similar detail. The study of the pH dependence has been extended to basic conditions, and the specific nature of the ions responsible for the cooperative salt effect has been clarified. Furthermore, protein constructs containing both domains have been studied in order to gain insight into the mutual interaction between the two domains when one or both are switched to the signal state.

Chapter 2 describes the preparation of the materials and all the experimental methods used in our work. Chapter 3 presents the results observed from the experiments. The decay time constants of the triplet state and the C(4a) Cysteinyl adduct were exhibited, and several factors effecting the photoreaction kinetics were also presented. Our knowledge acquired on the photocycle of the LOV2 domain is summarized in Chapter 4. In chapter 5, we discussed the experimental data and present models that can account for the details of the observed kinetics. Chapter 6 lists three kind of possible photoreaction schemes of the adduct formation and our inference according to our experimental results.

2 Materials and Experimental Methods

2.1 Phototropin from *Chlamidomonas reinhardtii*

2.1.1 Sequence

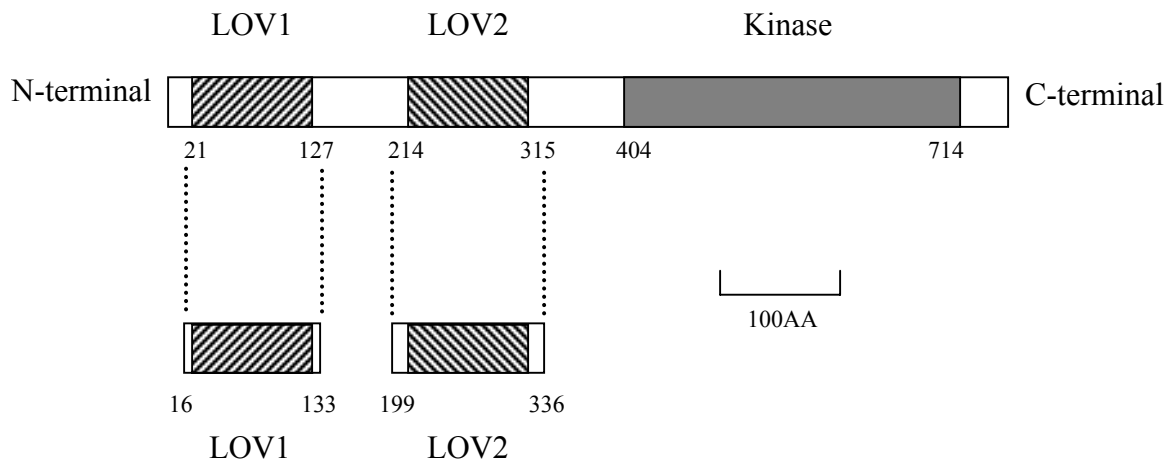


Figure 2.1. Schematic representation of the amino acid sequence in Phot1 of *Chlamidomonas reinhardtii* displaying the two LOV domains and the kinase domain.

In Phot of *C. reinhardtii*, the gene fragment of the sequences of amino acids (AA) from 21 to 127 belongs to LOV1 domain, and that from 214 to 315 is thought of as LOV2 domain (see the schematic representation in Figure 2.1). The molecular weight of Phot in *C. reinhardtii* is about 81 kDa, obviously smaller than the corresponding proteins from rice (~100 kDa) [40] or Arabidopsis (~120 kDa) [41]. A comparison of the amino acid sequences of Phot homologues revealed that the *C. reinhardtii* Phot protein has a distinctly shorter N-terminal end [29]. As

Materials and Experimental Methods

shown in Figure 2.1, there are only about 20 amino acids in front of the LOV1 domain. Other phototropins exhibit distinctly longer N-termini of rather variable amino acid composition [40]. During the preparation of LOV domains, usually about five more amino acids were kept at both terminals of them. For example, the LOV1 domain used in our experiments is the fragment from amino acid 16 to 133, not exactly from 21 to 127. Of these ~ 100 amino acids in each LOV domain core, 32 are fully conserved in the two LOV domains. Interestingly, this is not only the case for the LOV domains from *C. reinhardtii*, but also for other LOV domains from oat and fern [28]. This low divergence demonstrated between LOV1 and LOV2, also observed between lower and higher plants, indicates that the conserved regions are probably essential for the function of these domains.

2.1.2 Crystal Structure of LOV Domains

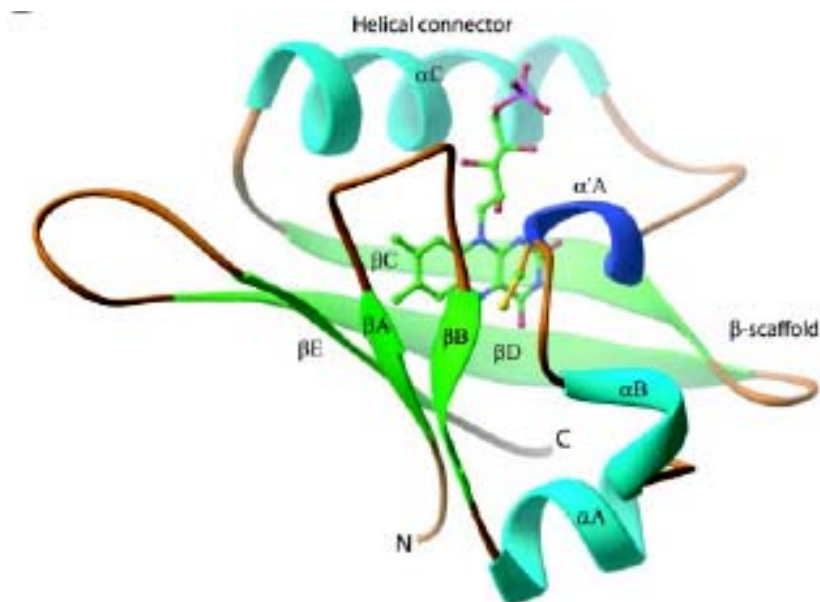


Figure 2.2. Ribbon diagram of the LOV2 structure from *Adiantum phy3* (PDB Nr.1g28)

Materials and Experimental Methods

The crystal structure of LOV2 from the fern *Adiantum* phy3-receptor in the dark form has been determined [42] and is shown in Figure 2.2. A single molecule of FMN is bound noncovalently in the interior of the LOV2 domain by a network of hydrogen bonds and van der Waals and electrostatic interactions. Importantly, the sulfur of a cysteine lies at a distance of ~ 4.2 Å from the C(4a) atom of the FMN chromophore. A direct comparison with the crystal structure of LOV1 from *C. reinhardtii* (PDB Nr. 1N9L) reveals no difference that can be seen only by inspection of the two figures. They are very similar, both from the exterior structure and the sequence of amino acids.

2.1.3 Comparison to other LOV-domain Sequences

Cr. LOV1: 21	TFVVADATLPDCPLVYASEGFYAMTGYGPDEVLGHNCRFLQEGETDPKEVQK	72
Cr. LOV2: 214	NFCISDPTLPDCPIVFASDAFLELTGYSREEVLGRNCRFLQAGTDRGTVDQ	265
At. LOV1: 198	TFVVS DATKPDYPIIMYASAGFFNMTGYTSKEVVGRNCRFLQSGTDADELAK	249
At. LOV2: 476	NFVITDPRLPDNPIIFASDSFLELTEYSREEILGRNCRFLQGPETDLTTVKK	527
Ac. LOV1: 676	SFIVVDALKPDFPIIYASTGFFNLTGYTSREVIIGNCRFLQGPDTNPADVAS	727
Ac. LOV2: 930	SFVITDPRLPDNPIIFASDRFLELTEYTREEVLGNNCRFLQGRGTRKAVQL	981
As. LOV1: 140	TFVVS D ASRPGHPIMYASAGFFNMTGYTSKEVVGRNCRFLQSGTDPAEIAK	191
As. LOV2: 417	NFVITDPRLPDNPIIFASDSFLQLTEYSREEILGRNCRFLQGPETDRATVRK	468
	* * * * *	
Cr. LOV1: 73	IRDAIKKGE-ACSVRLLN [*] YRKDGTPFWNLLTVTPIKTPDGRVSKFVGVQVDV	123
Cr. LOV2: 266	IRAAIKEGS-ELTVRILN [*] YTKAGKAFWNMFTLAPMRDQDGHARFFVGVQVDV	316
At. LOV1: 250	IRETLAAGN-NYCGRILN [*] YKKDGT [*] SFWNLLTIAPIKDES [*] GKVLKFIGMQVEV	300
At. LOV2: 528	IRNAIDNQT-EVTVQLIN [*] YTKSGKKFWNIFHLQPMRDQKGEVQYFIGVQLDG	578
Ac. LOV1: 728	IREALAQGTGTF [*] CGRLLN [*] YRKDGSSFWNLLTIAPIKDDLGSIVKLI [*] GVQLEV	779
Ac. LOV2: 982	IRDAVKEQR-DVTVQVLN [*] YTKGGR [*] AFWNLFHLQVMRDENGDVQYFIGVQ [*] QEM	1032
As. LOV1: 192	IRQALANGS-NYCGRVLN [*] YKKDGT [*] AFWNLLTIAPIKDEEGRVLKFIGMQVEV	242
As. LOV2: 469	IRDAIDNQT-EVTVQLIN [*] YTKSGKKFWNLFHLQPMRDQKGDVQYFIGVQLDG	519

Figure 2.3. Alignment of amino acid sequences of various LOV domains. The amino acids interacting directly with the FMN chromophore are marked with an asterisk. Residues are conserved in all LOV domains. Cr: *Chlamydomonas reinhardtii*; Ac: *Adiantum capillus-veneris*; At: *Arabidopsis thaliana*; As: *Avena sativa*

Materials and Experimental Methods

Figure 2.3 depicts the aligned sequences of amino acids in several LOV domains from different organisms which have been studied in recent years by many groups. The amino acids in the immediate neighborhood of the FMN chromophore have been identified and are marked by asterisks. In addition the amino acids conserved in all LOV domains are highlighted by bold print. It is remarkable that all amino acids in contact with FMN are identical in all domains.

These high homogeneities between their structures are in line with the observation that all LOV domains display qualitatively identical photocycles. Nevertheless, the slightly different protein surrounding of the FMN cofactor in LOV1 and LOV2 domains causes considerable differences in the kinetic characteristics of their photocyclic processes, as will be shown later. However, it is presently not possible to explain the different behavior of the various LOV domains on the basis of their amino acid sequences.

The amino acid sequences of LOV1 and LOV2 are always approximately 40% identical, whether within a given phototropin or between phototropins from different plant species [19]. The picture shown above can also illustrate this point. In addition, the amino acid sequence of the kinase domain of Phot1 of *C. reinhardtii* shows 60% similarity compared to Phot1 from *Adiantum capillus-veneris*, and 64% for Phot1 from *Pisum sativum*. Moreover, the sizes of the LOV domains (~ 100 amino acids) and the size of the kinase domain (~ 295 amino acids) are nearly the same in the *C. reinhardtii* protein and in the phototropins of other species [40]. Hence, the functions of the two LOV domains should be evolutionarily homologous, and although there are numerous differences between them which cause some quantitative distinction between their kinetic properties.

2.2 Protein Preparation

2.2.1 Wild-type

All proteins used in the experiments were prepared by Tina Schireis, department of biology, university of Regensburg. The full-length cDNA-clone (Acc. No: AV 394090) of the *C.reinhardtii* was received from C.F. Beck and K. Huang, university of Freiburg. The gene fragment coding for the FMN-binding LOV domains was amplified by PCR and inserted into the XhoI and *Bam*HI sites of the *E. coli* expression vector pET16 (Novagen, Bad Soden) in such a way that the protein N-terminally carries one Gly, 10 His, and a protease cleavage site (factor Xa). The protein was expressed in *E. coli* strain BL21 (DE3).

The gene fragment encoding the LOV domains were amplified by PCR using oligonucleotide primers that contain *Eco*RI and *Hind*III restriction sites. The PCR product was digested with *Eco*RI and *Hind*III and cloned into the pMalc2X or p2X – vector (New England Biolabs). The MBP-encoding segment was excised and the resulting vector was named p2X. A DNA sequence encoding 10-Histidines was inserted into the *Eco*RI site. Then the fusion protein was expressed in BL21 and purified via a nickel-nitrilotriacetic acid (Ni-NTA) column (Qiagen, Hilden) filled with agarose according to the instructions of the manufacturer.

The chromophore in LOV domains is FMN as determined by chromophore extraction in 1% TCA (Trichloroacetic acid), protein precipitation, and electrospray mass spectroscopy. For injection, the samples were diluted in 0.5% acetic acid, 50% acetonitrile. The determined molar mass of the apoprotein is $15,609 \text{ g mol}^{-1}$, which is 130 g mol^{-1} below the expected value ($15,739 \text{ g mol}^{-1}$), indicating that the N-terminal methionine was cleaved off in the mass spectrometer. The molar mass of 457 g mol^{-1} for the chromophore corresponds to that of FMN.

2.2.2 Mutants

Mutants were generated by site-directed mutagenesis and expressed by the same means as the wild-type proteins described above. In this thesis, several mutants have been used in which the reactive cysteine of a LOV domain is replaced by another amino acid (i.e. serine, glycine). For LOV1 this mutant is LOV1-C57S, the corresponding mutant for LOV2 is LOV2-C250S. In order to study the interaction between the two LOV domains, in addition to the tandem construct LOV1+2 also the two mutants LOV1+2-C57S and LOV1+2-C250S have been employed in which one of the two domains has been inactivated.

2.2.3 Purification

The protein was purified via Ni-NTA resins according to the instructions of the supplier (Quiagen, Hilden). Then it was dialyzed into pH8 buffer, containing 10 mM NaCl, 10 mM phosphate. Prior to the experiments, the samples were always diluted in a pH8 buffer, containing 10 mM phosphate and 10 mM NaCl.

2.2.4 Gel Chromatography

Gel chromatography is a technique for separating chemical substances by exploiting the differences in the rates at which they pass through a bed of a porous, semisolid substance. It is also called gel filtration. The standard substances, i.e. BSA (bovine serum albumin) 66 kDa, Carbonic anhydrase 29 kDa, Lysozyme 14.4 kDa and Vitamin B₁₂ 1.3 kDa, were dissolved in a pH 6.8 buffer, 0.1 M NaH₂PO₄, then taking 5.0 µl of it and injecting it onto a 300 × 7.8 mm BIOSEP-SEC-S3000 column (Phenomenex, USA), and then injecting the proteins 5.0 µl onto

the column. The temperature was kept at 25°C. It is empirically known that the transition time of a compound varies linearly with logarithm of the mass, with larger masses moving faster than smaller ones. Knowing the masses of the standard substances, the relation $t = a - b * \log (M)$, was used to calibrate the measurement.

2.3 Experimental Methods

2.3.1 Flash Photolysis

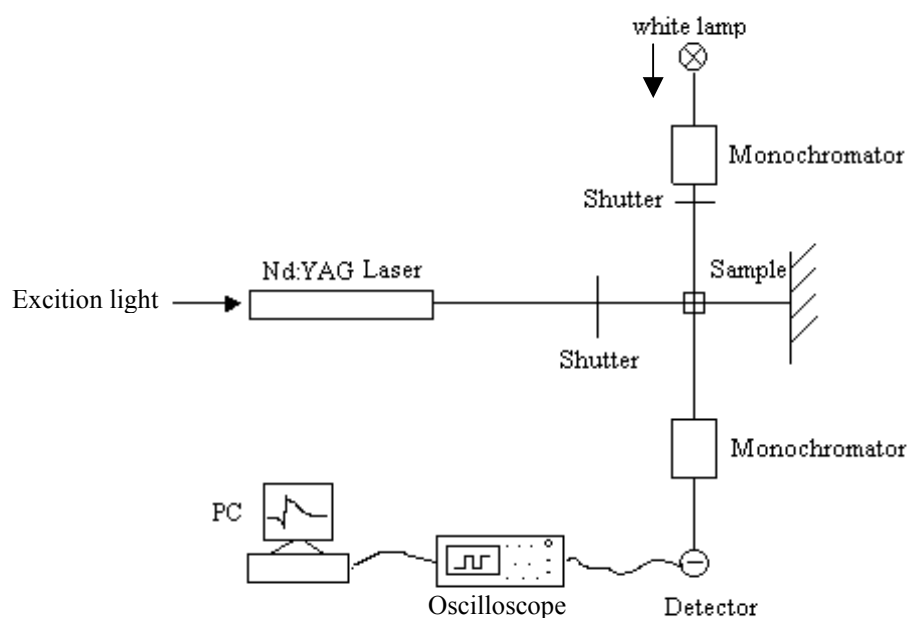


Figure 2.4. Schematic setup of Flashphotolysis experiment

Laser flash photolysis is a technique used to study short-lived, photochemically generated intermediates. Precursor molecules are irradiated by a laser pulse with a duration that is short enough to generate the intermediates of interest faster than their decay times. The intermediates

Materials and Experimental Methods

generated in this way are monitored to provide time-resolved and spectrally dispersed data. The above picture is the schematic diagram for our experiment setup.

In our work, the sample was placed into a rectangular cuvette and excited by a light pulse of 15ns duration, 5×10 mm cross section, and ~ 1 mJ energy from a Scanmate dye laser (Lambda Physik, Göttingen, Germany), which is pumped by the third harmonic of an SL-803 Nd:YAG (Spectron Laser Systems, Rugby, England). The dye coumarine 440 in ethanol was used to tune the laser wavelength to the maximum of the absorption band of FMN around 447 nm. The transient absorption was measured along the 10mm pathway perpendicular to the excitation using a pulsed 150-W Xe lamp (MSP-05, Müller, Moosinning, Germany). Two monochromators, one before and the other after the sample, were taken to select the wavelength and exclude fluorescence and stray light. The transmitted signal was detected by a R446 photomultiplier (Hamamatsu Photonics, Herrsching, Germany) and recorded by a 500-MHz digital storage oscilloscope (TDS 744A, Tektronix, Beaverton, OR, USA) triggered by the excitation pulse via a photodiode. A trigger generator regulated the selection of single laser shots from the 20-Hz pulse train of the laser and the synchronization of the experiment. Oxygen was removed from the sample through bubbling with argon for 30 min.

Each data set was created by taking four averaged traces in succession: the signal trace (I_S), the reference trace without laser (I_R), a fluorescence signal without measuring pulse (I_F), and a baseline without both light sources (I_B). The temperature was always kept at 20°C. The experimental data were converted to the transient change in extinction, $\Delta E(t)$, according to the following function:

$$\Delta E(t) = -\log \frac{I_S(t) - I_F(t)}{I_R(t) - I_B(t)} \quad (2.1)$$

These time traces could be fitted by the single- or double-exponential decay functions. All flash photolysis experiments were performed in the time range 100ns ~ 1ms. The transient absorptions observed at wavelengths between 650 nm and 750 nm are attributed to the triplet state of FMN.

2.3.2 UV/Vis Spectra

The absorption spectra were recorded with a Lambda 9 spectrophotometer (PerkinElmer, Frankfurt, Germany). The samples were kept in a rectangular (10 × 2 mm) cuvette. Following illumination by blue light source, the recovery time traces were recorded at 475 nm in the dark. During these measurements the temperature was maintained at 20°C by water circulation from a thermostate (Thermomix 1460, B. Braun, Germany).

Dependence of slow kinetics on pH and NaCl

Samples with different pH values and salt concentrations were obtained by adding 1M potassium phosphate buffer and 1M sodium chloride solutions into the standard samples. They were irradiated for 60s with a 50-W tungsten lamp (Osram, München, Germany) through a 435nm cutoff filter (GG435, Schott, Germany) and the subsequent recovery of the ground state monitored at 475 nm in 0.2 s intervals by the Lambda 9 spectrophotometer.

Replacement of Na⁺ and Cl⁻ by different cations and anions

The standard samples were dialyzed in a 10 M potassium phosphate buffer of pH4.7. Potassium chloride, N-methylglucamine chloride, tetraethylammonium chloride, sodium perchloride and sodium phenylsulfonate were added as a 1 M solution to a final concentration of 100 mM. The pH changed only slightly by the addition.

Varying NaCl concentration at acidic pH

Starting from a 10 mM or 100 mM potassium phosphate buffer at pH4.7, the NaCl concentration of the protein solution was varied from 5 to 600 mM by addition of 1M NaCl. The LOV1 domain used in the salt dependence and ions influence was connected to a His-pMal fusion protein.

Activation Energy of the LOV-390 decay

The temperature was set within the range 20 ~ 30°C and was stabilized with an accuracy of 0.1°C by water circulation from a thermostate. Time traces were recorded as described above.

Photochemical back-reaction

The samples were irradiated with visible light from a 100-W tungsten lamp or UV light (280 ~ 390 nm) from a Xe lamp. Bleaching $\Delta A/A$ of the absorption was monitored at 475 nm after reaching the photostationary state. Strong light pulses of ca. 1 s duration from two 1-W blue LEDs (light emitting diode) were used to saturate the photoreaction and obtain the limit bleaching of the absorption. The intensity of LED is much stronger than common tungsten lamps, and the emission is centered at 470 nm. This wavelength is close to the peak absorption of the first absorption band of FMN whereas the photoproduct LOV-390 has very little absorbance there. The emission spectrum of the blue LED was recorded with an MS 260i spectrograph (Oriel Instrument, Stratford, US) through a CCD camera (DH 720-18F-03, Andor, Germany). The transmission spectrum of the filter used for UV irradiation combination was checked with the Lambda 9 spectrophotometer.

2.3.3 Slow and fast Bleaching Kinetics

Slow bleaching measurements were performed with a 100-W tungsten lamp as photolytic light source. The samples were irradiated for 16 minutes with continuous blue light ($\lambda \geq 475$ nm). The absorbance at 475 nm during bleaching as well as the recovery after switching off the tungsten lamp was monitored with the Lambda 9 spectrophotometer. These experiments were repeated with different attenuator filters in front of the tungsten lamp. In a second set of experiments termed “fast bleaching experiments”, bleaching of the sample was achieved by intense flashes of two high-power blue LED of duration between 20 ~ 300 ms, and the recovery of the ground state monitored in the same way as in the “slow bleaching experiments”.

3 Results

3.1 Dark Form

3.1.1 UV-Vis Absorption Spectra

The absorption spectrum of the LOV2 dark form is shown in Figure 3.1. In order to compare it with other domains LOV1, LOV1+2 and the corresponding three mutants are also displayed in this picture. The spectrum of LOV2-C250S contained an obvious contribution from scattering, which was corrected for by subtraction of a contribution proportional to λ^{-4} . For a better comparison, the spectra are shifted vertically. Only minor differences in the spectra are visible. The absorption bands of all LOV domains are very similar: the $S_0 \rightarrow S_1$ transition has the strongest peak in the range 443 ~ 447 nm, with additional vibronic maxima near 470 nm and 420 nm. The $S_0 \rightarrow S_2$ transition appears as two vibronic bands of equal intensity with peak positions around 353 and 370 nm. Here S_1 is assigned to be the lowest singlet excited state of the protein-bound FMN chromophore, and S_2 is the higher singlet state of FMN. From these absorption curves, it is clearly exhibited that only a small shift of the main absorption peak is observed from 447 nm in LOV1 to 446 nm in LOV2, LOV1+2 and LOV1+2-C250S, to 444 nm in LOV1+2-C57S, and to 443 nm in LOV2-C250S. In addition, there are no significant shifts of these absorption bands observed by variation of the pH in the range 4.3 ~ 7.5 or the addition of salts up to a concentration of 600 mM. These spectral properties are consistent with LOV domains from *oat*, *Arabidopsis phot1*, and *Adiantum phy3* [19, 24, 43].

Results

Comparison of the absorption spectra of LOV1, LOV2, and LOV1+2 shows that the differences between them are quite small. Only the mutants, in which the reactive cysteine was replaced by serine, show a blue-shift of the main absorption peak. This has been reported for LOV1-C57S [30] and is very similar in LOV2-C250S, in which all peaks are a few nanometers blue-shifted. In the double domains with single mutations in one domain, the spectra of the two domains cannot be separated because of the complete overlap. The shift of the peak maximum is therefore the sum of the two contributing domains. Because of the high similarity, there is no evidence observed for any interaction between the two domains only from the absorption spectra.

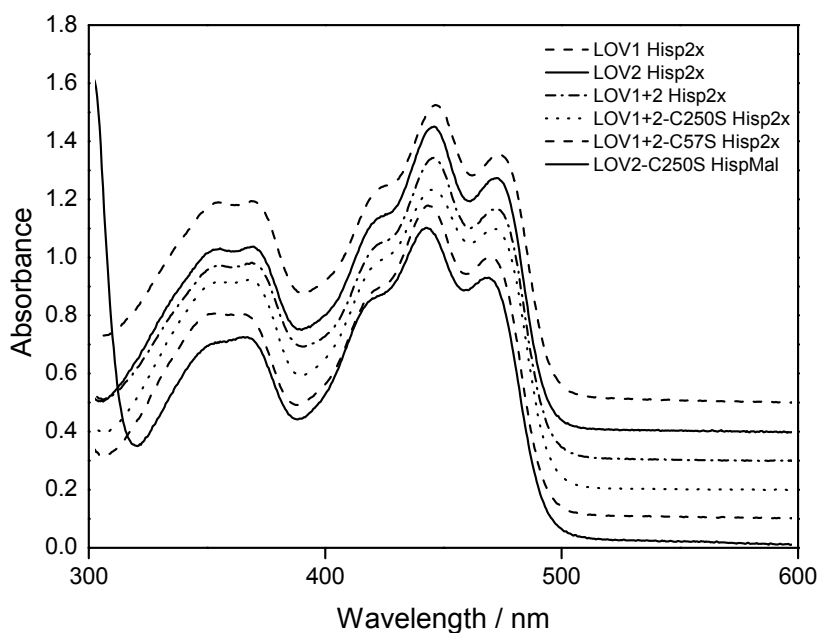


Figure 3.1. Absorption spectra of the investigated single and double LOV domain constructs

In addition, there is also no obvious difference observed from the spectra of other LOV1 mutants, including D31QR58K, Q120E, D31Q, R58K, D31N, which have been presented

previously in the literature [44]. This high similarity of the absorption spectra strongly indicates that the mutations do not influence the properties of the chromophore.

3.1.2 Stability on pH

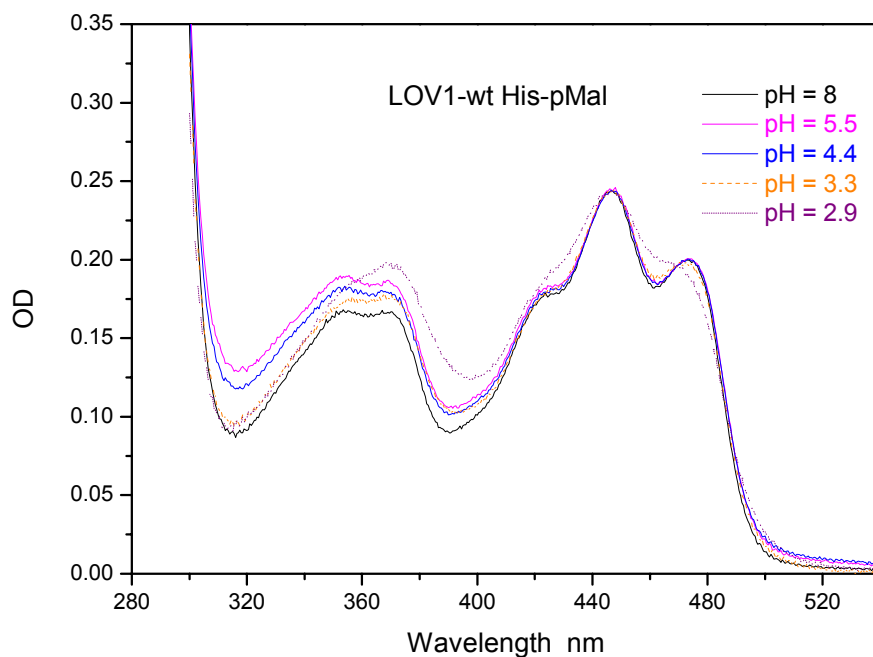


Figure 3.2. Absorption spectra of the wild-type LOV1 domain with different pH values

The stability of LOV1 and LOV2 samples in the dark form was investigated under acid conditions. The pH value was decreased through adding different amount of 1M phosphate buffer directly into the samples. In contrast to FMN bound by hydrogen bridges in the protein, free FMN shows a first absorption band with no vibrational substructure. Hence, from the variation of the spectra observed with decreasing pH, it is easy to obtain the pH range when the sample will be denatured. The results indicate that the LOV1 wild-type is a slightly more stable towards low pH than the mutants, and is much more stable than the LOV2 domain. Changes of

Results

the spectra of the LOV1 wild type with varying pH values are shown in Figure 3.2. Each spectrum's absorption peak at 447 nm was normalized to the spectrum of the standard sample. Apparently the sample was denatured gradually when the pH value is lower than 3.3. The LOV1 mutants, i.e. D31QR58K, Q120E, D31Q, R58K, D31N, would be denatured at ~ pH 4.0. The LOV2 domain displays much lower stability, since the characteristic loss of vibrational structure is already observed at pH 4.5.

In summary, the release of FMN occurs below pH 3.3 for the LOV1 domain, and below pH 4.5 in the LOV2 domain. This limits the range in which the kinetic properties of these domains can be investigated.

3.2 Triplet state

3.2.1 Decay of the triplet excited State

After excitation of the LOV domains to the excited singlet state with blue light, intersystem crossing into the triplet excited state occurs. This process has been investigated by ultrafast spectroscopy [43, 45]. This intermediate in the photocycle has a strong absorption in the spectral range of 650 to 715 nm [23, 30]. The LOV2 domain from *C. reinhardtii* Phot was studied here for direct comparison with known data on LOV1 from the same protein [30].

The decay kinetics of the triplet states was measured for the single LOV1 and LOV2 domains as well as the inactivated LOV2 domain, the LOV2-C250S mutant. In order to obtain information on the interaction of the two domains LOV1 and LOV2, the double domain construct LOV1+2 was also employed as well as two mutants, LOV1+2-C57S and LOV1+2-C250S. In LOV1+2-C57S the thiol group of the reactive cysteine in LOV1 is replaced by the nonreactive hydroxyl group of serine, in LOV1+2-C250S the corresponding exchange has been

Results

made in the LOV2 domain. Hence in these mutants, the adduct formation is selectively inactivated in one of the two domains. For easier comparison and analysis, all domains contained a His-p2x tag with the exception of the LOV2-C250S mutant and the wild-type LOV2 used in flash photolysis, which were available only as a His-pMal fusion protein.

Flash photolysis experiments were performed to determine the decay kinetics of the triplet excited state in the LOV2 domain (His-pMal). In analogy to the LOV1 domain, the triplet state of LOV2 is named LOV2-715 in the following. As depicted in Figure 3.3.A, LOV2-715 decays with a time constant of about 500 ns. The residuals (difference between spectral data and calculated data from exponential fitting) were within the noise level in the data. The strong fluorescence of the sample with a quantum yield of 7% [46] can easily saturate the photomultiplier. This interferes with the data acquisition in the first 100 ns even at the detection wavelength of 710 nm. Therefore the data in the first 100 ns are not accurate enough to permit a more detailed analysis of the decay.

In mutants of the LOV domains, where the reactive cysteine is replaced by alanine or serine, the lifetime of the triplet state increases significantly [23, 30]. In these mutants the adduct is not formed, therefore the lifetime of the triplet state is limited by other processes like intersystem crossing into the ground state or quenching by oxygen. These processes should also take place in the wild type and compete there with adduct formation. In the LOV2-C250S mutant (His-pMal), the lifetime of the triplet state is unusually long: Under aerobic conditions a biexponential decay with two time constants of 12 (± 3) μs and 287 (± 13) μs is observed (see Figure 3.3.B). The long time constant contributes 90% to the amplitude of the decay. To exclude the presence of a radical species or a charge transfer complex at the measuring wavelength of 650 nm, the experiment on the aerated sample was repeated with detection at 715 nm where only the triplet state is expected to absorb. At this wavelength the signal-to-noise

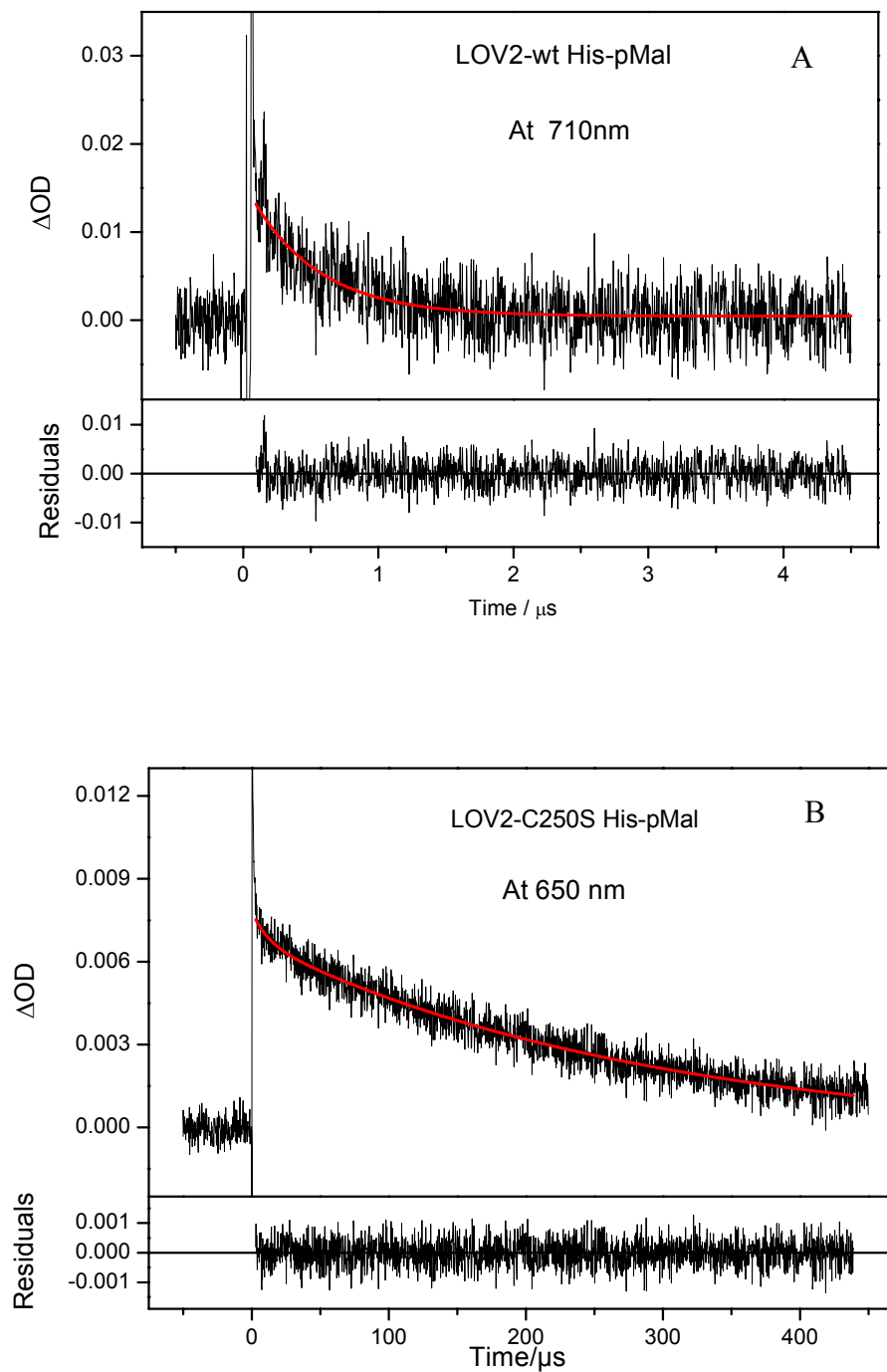


Figure 3.3. Decay time traces of triplet states of the wild-type LOV2 domain at 710 nm (A) and the mutant LOV2-C250S at 650 nm (B) after excitation with a blue laser pulse. Fitted curves are indicated with solid lines.

Results

ratio of our apparatus is smaller than at 650 nm. Taking this limitation into account, the decay times and amplitudes obtained from the data measured at 710 nm (not shown), $4 (\pm 1) \mu\text{s}$ (35%) and $256 (\pm 12) \mu\text{s}$ (65%), can be attributed to the same species observed at 650 nm. As we know, a solvent in contact with air normally contains sufficient dissolved oxygen to have an apparent effect on the decay kinetics of any solute triplet state [47]. We deduce that molecular oxygen could be a quencher when it is present close to the chromophore FMN in a certain fraction of the protein sample. So a sample bubbled with argon for 30 min was probed without oxygen. It shows a monoexponential decay with a time constant of $278 (\pm 3) \mu\text{s}$. The fast component has disappeared, which means that oxygen has an obvious effect on the decay kinetics of the short-lived intermediate LOV-715. So we attribute the faster decay component ($12\mu\text{s}$) to static quenching by oxygen.

In the double domain constructs, the triplet state lifetimes and the reaction rates for adduct formation in the excited domain might change by the presence of the second domain. The decay of the triplet excited state in the LOV1+2-C57S mutant was studied to investigate this influence. Because one domain cannot be excited selectively due to the complete overlap of the absorption spectra of the tandem two domains, a superposition of the two decay processes was observed. The decay process was fitted with a sum of three exponential functions resulting in time constants of 400 ns, $5 \mu\text{s}$ and $30 \mu\text{s}$ (see Figure 3.4.B). These values are close to those from the processes in the individual domains, which are 500 ns for wild-type LOV2 and $3 \mu\text{s}$ and $27 \mu\text{s}$ for the LOV1-C57S mutant [30]. An analogous experiment was performed with the LOV1+2-C250S mutant, where the adduct formation is inactivated in the LOV2 domain. In Figure 3.4.A, the time trace is depicted together with a biexponential fit with time constants of $4 \mu\text{s}$ (21%) and $253 \mu\text{s}$ (79%). A second measurement with a shorter time window showed two

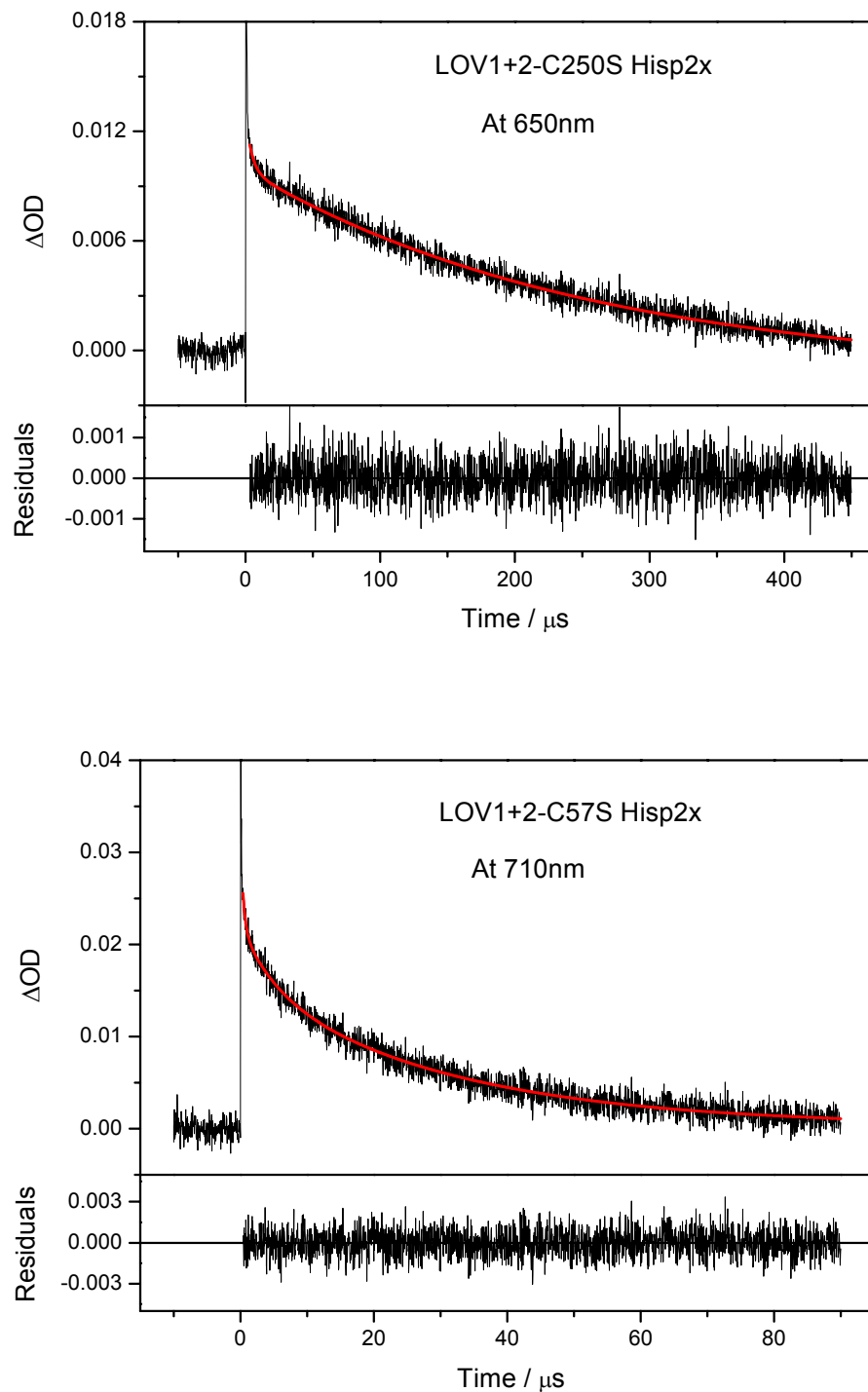


Figure 3.4. Decay time traces after excitation of the double domain constructs LOV1+2-C250S (A) and LOV1+2-C57S (B)

Results

time constants of 600 ns (82%) and 4 μ s (18%) (data not shown). Taken together, these time constants are similar to a superposition of the decay processes of LOV2-C250S mutant (\sim 12 μ s, \sim 290 μ s) and wild-type LOV1 (800 ns, 4 μ s) [30]. A summary of the triplet decay times is shown in Table 3.1.

Table 3.1. Time constants of the triplet state decay in the single and double LOV domains^a

Species	Time constant τ_1 (μ s)	Time constant τ_2 (μ s)	Time constant τ_3 (μ s)
LOV2	0.5	-	-
LOV2-C250S	-	12	287
LOV1+2-C250S	0.6	4	253
LOV1+2-C57S	0.4	5	30
LOV1 ^b	0.8	4	-
LOV1-C57S ^b	-	3	27

^a at pH 8, 10 mM NaCl and 20 °C. ^b Taken from reference Kottke et al. 2003

According to the previous measurement, we know the triplet excited state in the wild-type LOV2 domain from *C. reinhardtii* Phot decays with a time constant of 500 ns. Up to now, the lifetime of the triplet excited state has been investigated in two other LOV domains by time-resolved absorption spectroscopy: In LOV2 from *A. sativa* phot1, the wild-type domain shows a monoexponential decay with a time constant of 4 μ s [23], whereas in LOV1 from *C. reinhardtii* Phot, a biexponential decay is observed with 800 ns and 4 μ s [30]. Therefore, the LOV2 domain from *C. reinhardtii* Phot displays the fastest triplet state decay of the three domains, which might be an indication for a very efficient formation of the adduct in this domain.

Results

The triplet excited state in the LOV2-C250S mutant shows a decay with a main time constant of 250 to 300 μ s. Compared to the LOV1-C57S mutant with a main time constant of 27 μ s [30], ISC to S_0 takes significantly longer. For free FMN in phosphate buffer, a similar time constant of 204 μ s was determined from extrapolation to infinite dilution [48]. In the protein, triplet-triplet annihilation and quenching by FMN in the ground state are prevented by the protective cover of the apoprotein. The protein scaffold also reduces the contribution of low-frequency modes, as evidenced by the resolved vibrational structure in the UV spectrum. This may explain the long lifetime of the triplet state in LOV2-C250S. Still the question remains, what structural differences lead to a difference of a factor of 10 between the lifetimes of the triplet states in LOV1 and LOV2.

As stated formerly, the time constants of the decay of the triplet excited state in LOV1 and LOV2 do not change strongly if a second domain is present in the double domain construct. The triplet excited states in the LOV1+2-C57S as well as the LOV1+2-C250S mutant show a decay that can be interpreted as a simple superposition of the separate decays of LOV2 wild type combined with LOV1-C57S mutant and LOV1 wild type combined with LOV2-C250S mutant respectively. As a conclusion, the interaction between the two domains does not influence the properties of the triplet excited states of their chromophores.

On the basis of earlier molecular orbital calculation, this triplet excited state is the presumed reactive species that leads to adduct formation [42, 23]. Also no spectroscopically distinguishable intermediates precede the FMN triplet on the femtosecond to nanosecond time scale, which indicates that it is formed directly via ISC from the singlet state [43].

In addition, comparison to the free FMN in solution shows that the protein environment of LOV domains increases the reaction rate of FMN from S_1 to T_1 by a factor of 2.4, thereby

improving the yield of the cysteinyl-flavin adduct and the efficiency of phototropin-mediated signaling processes [43].

3.3 Decay of the Adduct

3.3.1 Decay Kinetics

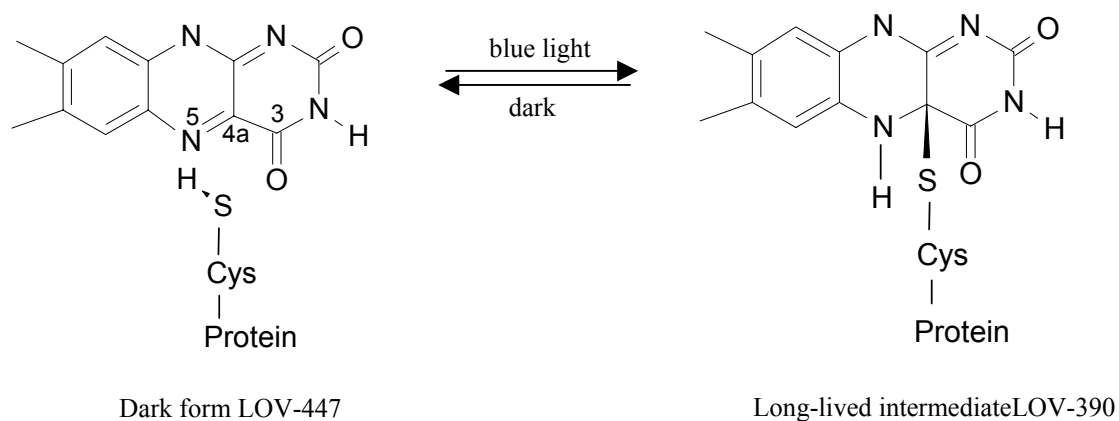


Figure 3.5. Schematic diagram of the formation of the flavin C(4a)-thiol adduct in LOV domains

The first absorption band of the dark form of LOV domains has a maximum at about 447 nm with two vibronic bands at 425 and 475 nm. There is a second broad absorption band around 350 nm. In the photocycle of the Phot-LOV domains, a long-lived intermediate is formed. This has been identified as the adduct formed between the carbon atom C(4a) of flavin and the cysteine sulfur [24, 25]. Formation of the cysteinyl-flavin adduct results in a loss of the blue absorption band and leads to an absorption peak at 390 nm. Hence the metastable intermediate is usually named LOV-390. This adduct reverts completely to the ground state in darkness. The schematic diagram is showed as Figure 3.5. The reactive N5 and C(4a) atoms are highlighted

Results

on the dark form molecule. Figure 3.6 shows the spectra of these species: the solid line is the spectrum of the dark form LOV-447, the dotted line is that of the adduct form LOV-390.

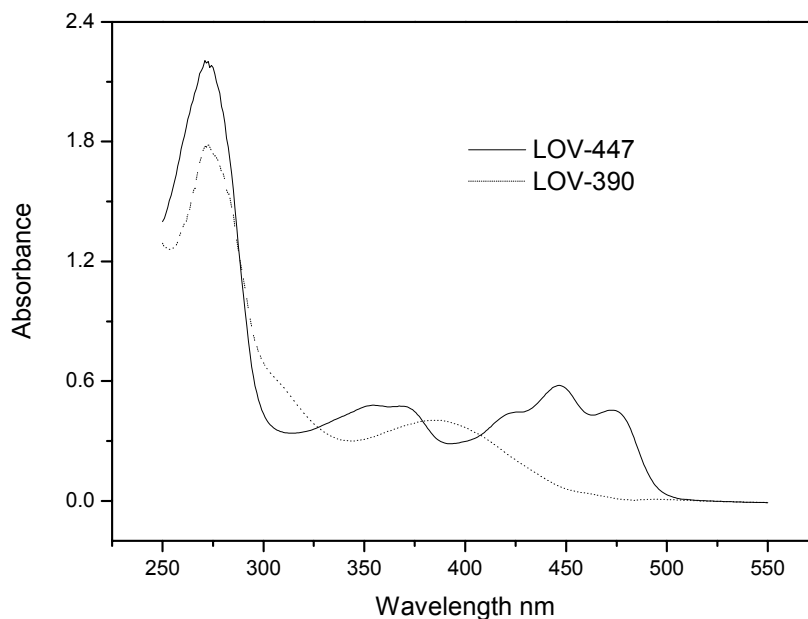


Figure 3.6. Spectra of the dark form (LOV-447) and adduct form (LOV-390) of the LOV domain

The decay of this adduct in the dark was monitored by measuring the recovery of absorption of the dark form at 475 nm following irradiation of the sample with a 50-W tungsten lamp for 60 seconds. Figure 3.7 displays a typical kinetic trace from the LOV1 domain. In many cases this decay time trace (recovery part) could be fitted by the monoexponential function

$$y = A_1 \cdot \exp(-t / \tau) + y_0 \quad (3.1)$$

This leads to the assignment of a characteristic time constant (τ) to this species. In many cases, however, a monoexponential function did not result in a good fit. Then a biexponential fit with the function

$$y = A_1 \cdot \exp(-t/\tau_1) + A_2 \cdot \exp(-t/\tau_2) + y_0 \quad (3.2)$$

was tried, leading to two time constants and two amplitudes. This could indicate the presence of two species with the characteristic time constants τ_1 and τ_2 and population ratio A_1/A_2 , but the underlying mechanism might be more complicated. This will be discussed in more detail in chapter 5.

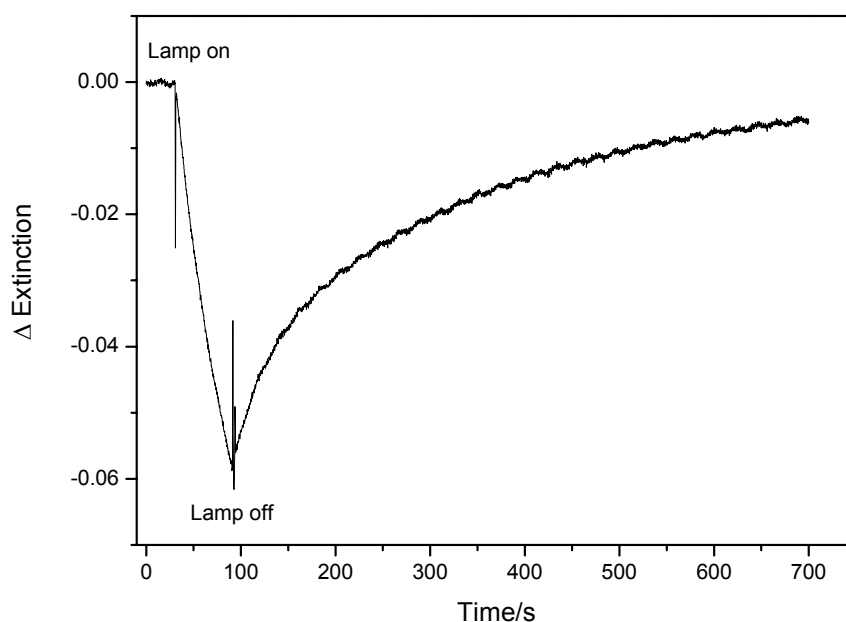


Figure 3.7. Recovery absorption changes of LOV domains monitored at 475nm with a 50-W tungsten lamp for 60 s.

In LOV2, the adduct decay cannot be fitted adequately by a monoexponential function. A biexponential fit produces two time constants of 30 s (25%) and 270 s (75%). LOV2 connected to a pMal fusion protein also showed a biexponential adduct decay with two time constants of 41 s and 387 s [46], but the different temperatures and illumination conditions make a direct comparison difficult. In contrast, the time traces of both mutated double domains are fitted

Results

adequately by a monoexponential function. Motivated by this observation, the adduct decay of the LOV1 domain was reinvestigated, which had been analyzed previously by a single exponential decay with a time constant of 200 s [30]. Indeed, a biexponential analysis revealed a small contribution (15%) of a fast decay component also in LOV1, resulting in time constants of 45 and 320 s.

Table 3.2. Time constants of the adduct decay in the single and double LOV domains^a

Species	Time constant τ_1 (s)	Time constant τ_2 (s)
LOV1	45 (15%)	320 (85%)
LOV2	30 (25%)	270 (75%)
LOV1+2	25 (30%)	270 (70%)
LOV1+2-C250S	-	260
LOV1+2-C57S	30	-

^a at pH 8, 10 mM NaCl and 20 °C. All domains were obtained from a Hisp2x construct.

For wild-type LOV1 from *C. reinhardtii* Phot, decay times of 168 s [37] and 200 s [30] have been reported. A similar value was also obtained from the measurements of ours, when the slight biexponentiality of the decay is neglected. For wild-type LOV2, there is a discrepancy between our values of 30 and 270 s and previous data with a 20 s decay time [37]. This difference may be related to the fact that our construct contains only a His-tag attached to the protein, whereas Kasahara et al. used a much larger calmodulin-binding protein. Interestingly, the LOV1+2-C57S mutant, in which the LOV1 domain is inactivated, shows a similarly fast decay time of 30 s. This is a clear indication of some interdomain interaction which blocks the slow pathway of adduct decay observed in the LOV2-His protein. The same observation applies

Results

also to the LOV1-His domain and the LOV1+2-C250S mutant. The comparison shows that the LOV1 domain has in this respect a stronger influence on LOV2 than vice versa. The influence on the adduct decay in the first domain is exerted without light activation of the second domain. However, the molecular basis for the observed biexponentiality in LOV1-His and LOV2-His is not yet understood.

The wild-type LOV1+2 double domain shows an adduct decay, which can be interpreted simply as a superposition of the decays of two single domains in the LOV1+2 mutant systems. The values of 260 s and 30 s are in fair agreement with previous measurements [37].

The present results are consistent with the hypothesis that the Cysteine is essential for the photocycle [24]. The investigation of the kinetic properties of the adduct decay in the S-mutated double domains, LOV1+2-C250S and LOV1+2-C57S, also supports this hypothesis. The wild-type LOV domains perform their photocycles many times without any detectable change in their absorption properties. However, it is found that there are several factors influencing the process of the adduct decay, such as pH, salt, and temperature. How they affect this process will be studied in more detail in the following part.

3.3.2 pH Effect

In the single LOV1 domain a strong pH effect on the adduct decay has been described. When the pH is lowered from 8.0 to 3.8 in the single LOV1 domain, the amplitude of the fast decay component quickly disappears and the decay becomes essentially monoexponential. The decay time of this process increases from 280 s at pH 6.8 to 860 s at pH 3.8 [30]. For the LOV2 domain, however, two decay components are observed in the whole pH range 4.7 ~ 10.0. The amplitude of the fast component increases under acidic conditions, from 16 % at physiological

Results

pH 7.5 to 38% at pH 4.3. The pH dependence of the two time constants of the biexponential decay are plotted separately in Figure 3.8.A. Whereas the time constant of the faster decay is not affected, that of the slow decay increases by a factor of 3.5 in going from neutral to acidic conditions. In the range pH 7-10 it is almost constant. In contrast to LOV1, an increase of the NaCl concentration from 10 mM to 100 mM does not alter the pH-dependence of the life times. Due to release of the chromophore, LOV2 could not be studied at lower pH than 4.7. Hence a second plateau in the pH dependence could not be observed. The model has been used to explain the pH-dependence of the decay time for LOV1 [30].

This model assumes that the system can exist in a protonated form BH and the corresponding base B⁻. Each of the two forms, BH and B⁻, decay back to the ground state with a characteristic rate constant k_1 and k_2 , respectively. When the equilibrium between both forms is established much faster than both k_1 and k_2 , a monoexponential decay is observed with the apparent rate constant:

$$k = k_1x + k_2(1 - x) \quad (3.3)$$

Here x is the mole fraction of the protonated form, which is related to the concentration ratio by:

$$\frac{[B^-]}{[BH]} = 10^{pH - pKa} = \frac{1 - x}{x} \quad (3.4)$$

This leads to the following equation, which is the pH dependence of the time constant:

$$\tau = \frac{1}{k} = \frac{10^{(pH - pKa)} + 1}{10^{(pH - pKa)} k_2 + k_1} \quad (3.5)$$

Results

The adduct decay in the LOV2 domain displays a similar pH dependence as in LOV1 (see Figure 3.8.A). So it could also be explained by the model described above. But a reliable fit using this acid-base model [30] is not possible since the pK_a value of the acid/base pair is too close to the limit of the pH stability range of LOV2 near pH 4.5. Therefore only an estimate of $\tau > 1400$ s can be obtained. The equilibrium constant pK_a is within the range of 5 ~ 6. The corresponding theoretical curve is also shown in Figure 3.8.A. This value is quite similar to the pK_a values 5.3 and 5.6 found in LOV1 domain with 10 mM and 100 mM NaCl. The chemical nature of this acid/base pair has not yet been identified. It might be related to the arginine Arg58 which is involved in the binding of the phosphate group of FMN through hydrogen bonds. This arginine in direct neighborhood to the reactive cysteine is conserved in LOV2 (Arg251) [21].

Interestingly, there is a big difference between LOV1 and LOV2 domains. In LOV1 domain, the adduct decay becomes monoexponential at pH ≤ 7.5 and the fast component disappears, but the decay of LOV2 is biexponential in the whole range. In order to get more information, we checked the double domain, LOV1+2-C57S, which contains a wild-type LOV2 domain and an inactivated LOV1 domain. A change of the pH value has no significant effect on the recovery of the dark form (see Figure 3.8.B). The decay remains monoexponential with nearly constant decay time in the pH range 4.3 ~ 7.4. In addition, no significant change is observed when the NaCl concentration is increased from 10 mM to 100 mM. The values and the pH effect in the LOV1+2-C57S mutant are in the same range as those of the fast component of the wild-type LOV2 decay curves, whereas the slow component is completely absent. This result might be due to a coverage of the protonation site in LOV2 by the attached LOV1 domain, suggesting an interaction between LOV1 and LOV2. In LOV2 from *A. sativa* phot1 the effect of pH change

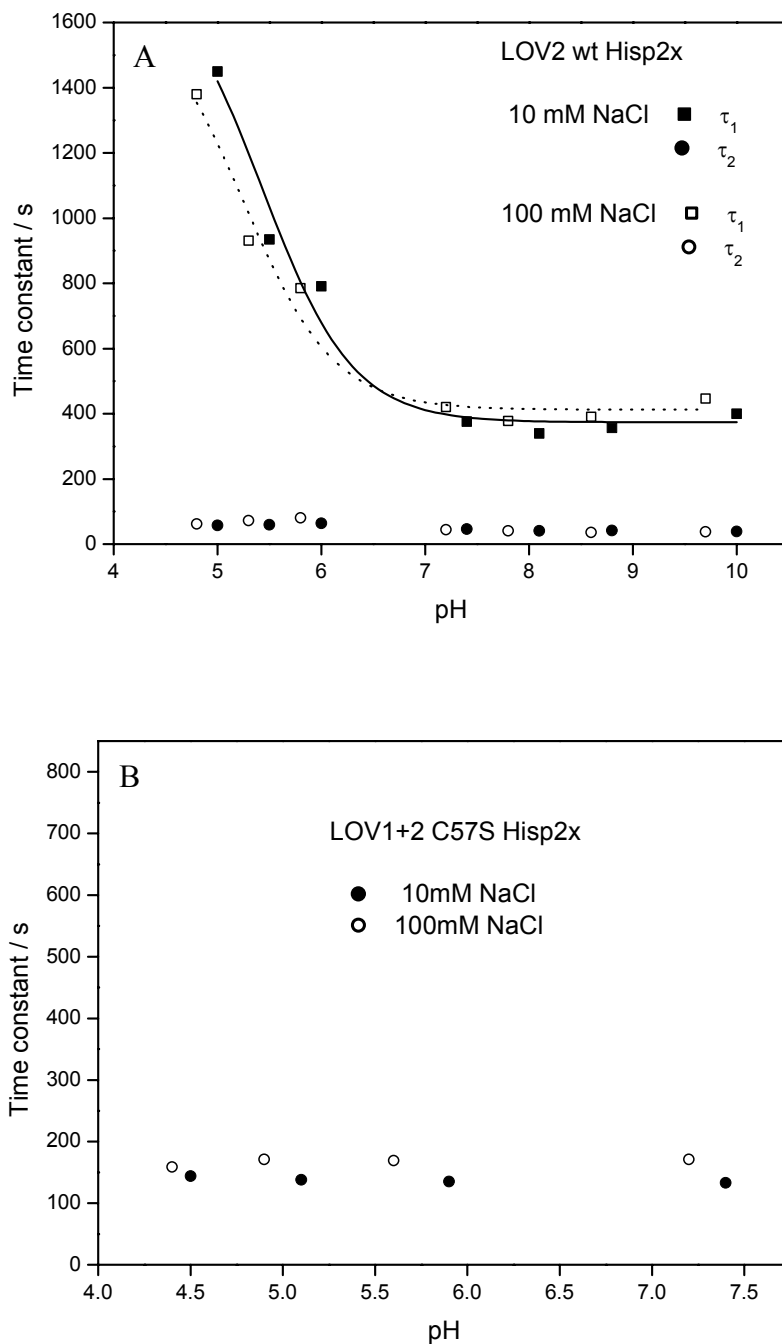


Figure 3.8. pH dependence of the time constants obtained from the adduct decay in the LOV2 domain at 10 and 100 mM NaCl concentration and 100 mM phosphate buffer. (A) The two time constants of the biexponential decay in the wild-type LOV2 are plotted separately. (B) In the LOV1+2-C57S mutant only the LOV2 domain is forming the adduct.

Results

on the adduct decay time is small [49]. Again, this might be explained by the fact that calmodulin-binding protein was used as fusion protein.

In addition, the pH effect was also investigated under basic conditions. In both LOV1 and LOV2 single wild-type domains, the decay time traces were always biexponential. The fast component of the decay remains almost constant and shows little effect by pH. However, the slow component displays a slight dependence on basic pH in LOV1 domain in contrast to LOV2, for which the pH value nearly has no influence on the adduct decay. In LOV1 the time constant increases again when the pH value increased, again in contrast to the behavior of the other domain.

The pH dependence for the slow decay constant of LOV1 is plotted in Figure 3.9 for the whole range (pH 4 ~ 10) studied. We can simulate this behavior by extending the system discussed in the previous section to three forms, BH_2^+ , BH and B^- . Each of these forms decays back to the ground state with a characteristic rate constant k_1 , k_2 and k_3 , respectively. We assume that these forms are in equilibria:



The relation between the concentration ratio and the equilibrium constant, K_{a1} or K_{a2} , exhibits as the following:

$$\frac{x_1}{x_2} = \frac{[BH]}{[BH_2^+]} = 10^{pH-pK_{a1}}, \quad \frac{x_3}{x_2} = \frac{[B^-]}{[BH]} = 10^{pH-pK_{a2}} \quad (3.7)$$

and
$$x_1 + x_2 + x_3 = 1 \quad (3.8)$$

Results

If the equilibrium between these forms is established much faster than their decays, the apparent decay rate constant is the average of the three decay constants weighted with the three mole fractions:

$$k = \frac{1}{\tau} = [BH_2^+] * k_1 + [BH] * k_2 + [B^-] * k_3 = 1 \quad (3.9)$$

the above relations leads to the following equation:

$$\tau = \frac{10^{pKa1+pka2} + 10^{pH+pKa2} + 100^{pH}}{k_1 * 10^{pKa1+pka2} + k_2 * 10^{pH+pKa2} + k_3 * 100^{pH}} \quad (3.10)$$

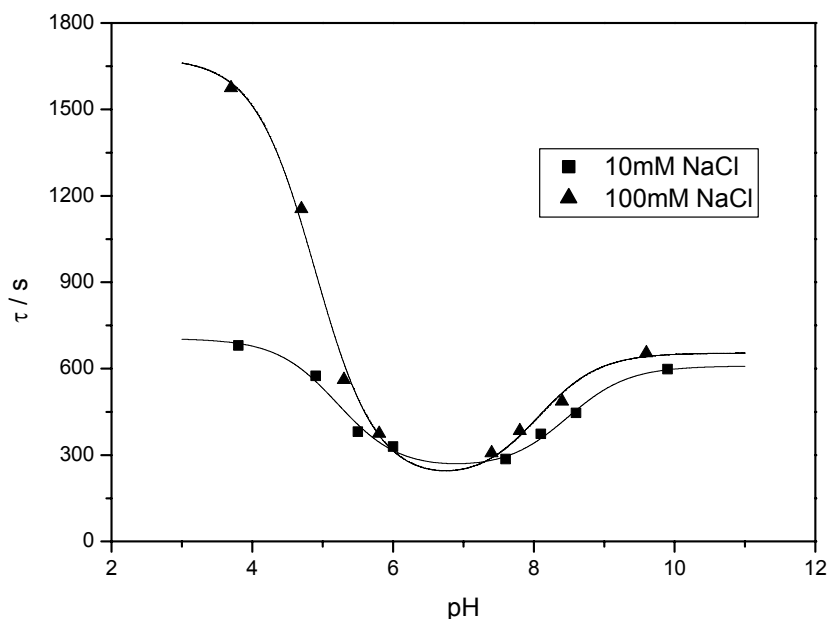


Figure 3.9. pH dependence of the time constants obtained from the adduct decay in the LOV1 domain at 10 and 100 mM NaCl concentration and 100 mM phosphate buffer

In Figure 3.9, the curves show the fit of equation (3.10) to the data points. A comparison of these experimental points with the similar experiment performed previously by Kottke, but only

Results

up to pH = 8, reveals no much obvious difference. The pKa values obtained by fitting with the pH-dependence equation in the acidic range are 5.7 and 5.8 for the samples containing 10 mM NaCl and 100 mM NaCl, respectively, in good agreement with the values 5.3 ~ 5.6 found by Kottke. With the extended data set, a second pKa value can be obtained in the basic range (7 ~ 10) by the fitting. In this case this is 7.5 and 8.0 for the samples containing 10 mM NaCl and 100 mM NaCl, respectively. This might indicate the deprotonation of the FMN-phosphate at this pH value leading to a change in the interaction between FMN and some amino acids around FMN.

3.3.3 Influence of NaCl Concentration

Table 3.2. Influence of cations and anions on the time constants of the adduct decay in LOV1^a

Cation varied		Time constant(s)	Anion varied		Time constant(s)
Na ⁺	Cl ⁻	692	Na ⁺	Cl ⁻	692
NMG ⁺	Cl ⁻	659	Na ⁺	ClO ₄ ⁻	397
K ⁺	Cl ⁻	645	Na ⁺	(C ₆ H ₅)SO ₃ ⁻	341
(Et) ₄ N ⁺	Cl ⁻	622			

^a at pH 4.7, 10 mM phosphate buffer and 100 mM ion concentration. The LOV1 domain was obtained from a His-pMal construct.

The increase of the adduct lifetime of LOV1 under acidic conditions is strongly amplified by a simultaneous increase of the NaCl concentration from 10 mM to 100 mM [30]. A similar behavior was not observed in the LOV2 domain or the mixed domain LOV1+2-C57S mutant. In LOV2 this effect is much weaker, as can be seen in Figure 3.8.A. In the LOV1+2-C57S mutant, the NaCl concentration has a small and constant effect in the whole range from pH 4 to

Results

7 (see Figure 3.8.B). Hence a specific interaction of LOV1 with either sodium or chloride ions might be present. Sodium and chloride were therefore replaced by cations and anions of more delocalized charge and bigger size. Measurements were performed in a 10 mM phosphate buffer at pH 4.7 and 100 mM salt concentration in all cases for direct comparison. Replacement of sodium by the cations potassium (K^+), N-methylglucamine (NMG^+), or Et_4N^+ slightly reduces the time constant by 5 ~ 10 % (Table 3.2). Replacement of chloride by the anions perchlorate (ClO_4^-) or phenylsulfonate ($C_6H_5SO_3^-$), however, drastically reduces the lifetime of the adduct by almost 50 % and brings it back close to the value observed for low salt concentration (10 mM). Hence we conclude that of all ions investigated the chloride ions have by far the strongest influence on the decay time of the adduct.

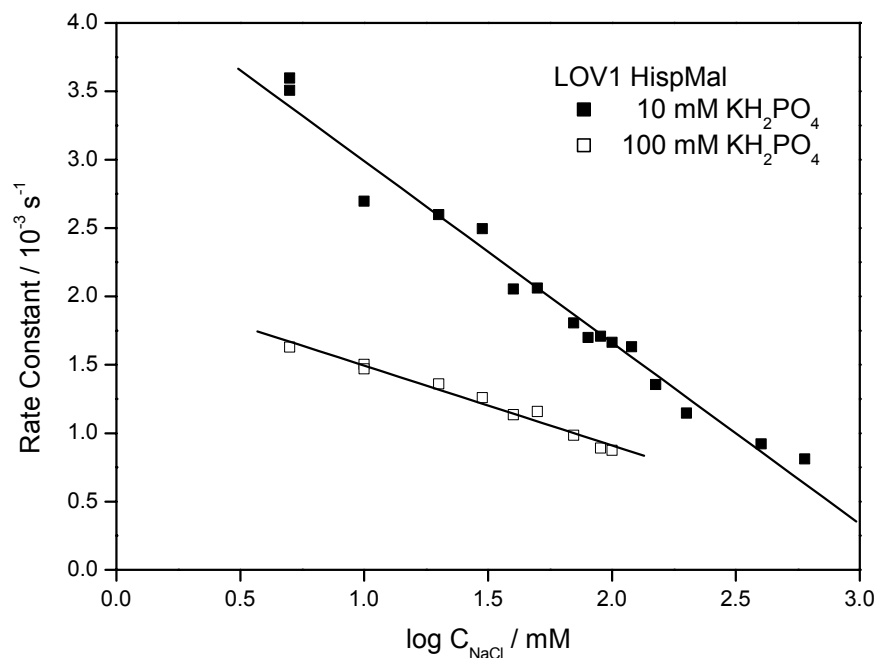


Figure 3.10. Rate constants of adduct decay in the wild-type LOV1 domain at 10 mM and 100 mM phosphate buffer pH 4.7. The NaCl concentration was varied from 5 to 600 mM. The logarithmic representation yields a linear dependence.

Results

If new species induced by increased salt concentration are in fast equilibrium with the species observed at low salt concentration, a monoexponential decay will be observed. If the new species induced by high salt concentration have well defined stoichiometry, a stepwise dependence of the rate constant on the salt concentration is expected, with each step corresponding to an equilibrium. In search of a defined stoichiometry of the interaction between LOV1 and chloride ions, the dependence of the adduct decay on Cl^- was studied as a function of NaCl concentration in the range from 5 to 600 mM in phosphate buffer solutions of 10 and 100 mM pH 4.7 (see Figure 3.10). However, the concentration dependence shows no steps that could be interpreted in terms of equilibria between FMN and $\text{FMN}\cdot\text{Cl}_n$ complexes with a defined stoichiometry. Instead a linear rise of the rate constant with the logarithm of the salt concentration is observed. Therefore, a specific interaction of chloride with a single site, e.g. by intrusion of a chloride ion into the binding pocket of the FMN, is unlikely. Such a specific interaction between a chloride ion and a serine has been identified within the chloride pump halorhodopsin [50].

The smooth logarithmic dependence on the chloride concentration observed for the rate constant of LOV1 suggests an unspecific interaction that gradually weakens the driving force and/or increases the barrier for the thermal back reaction of the adduct. The FMN in the dark form of the LOV domains is held in place not by a covalent bond but by ca. 15 hydrogen bonds to amino acid side chains [28]. The X-ray structure of the adduct shows that most of these hydrogen bonds are changed by the formation of the cysteinyl adduct. This might contribute to the driving force for the thermal back reaction. Chloride ions might modify the electrostatic potential near these hydrogen bonds, especially in the vicinity of the solvent-accessible phosphate group of the FMN. A mutation of R58K (arginin R was replaced by lysine K), which contributes with 2 hydrogen bonds to fixation of the FMN phosphate to the protein in LOV1,

Results

has indeed shown a profound influence on the velocity of the thermal back reaction [44]. This conservative mutation does not alter the hydrogen bonding network strongly, as the effects of pH and NaCl on the adduct decay are still present (see Figure 3.11.). And the equilibrium pKa values, for 10 mM and 100 mM NaCl concentration respectively, are still the same as those of the wild-type LOV1.

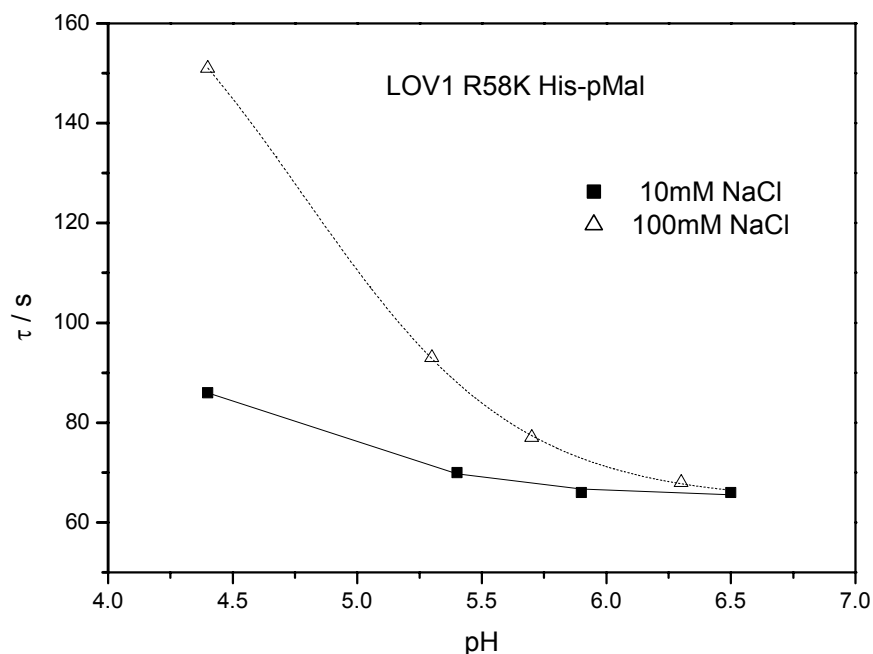


Figure 3.11. pH dependence of the time constants obtained from the adduct decay in the mutant LOV1-R58K at 10 and 100 mM NaCl concentration and 100 mM phosphate buffer.

3.3.4 Activation Energy of Bond Cleavage in the Adduct

In many cases the temperature dependence of rate constants of reactions can be analyzed in terms of the Arrhenius equation:

$$\ln(k) = \ln(A) - E_a/RT \quad (3.11)$$

Results

where k is the reaction rate constant (reciprocal of time constant τ), A is a constant (frequency factor), E_a is the activation energy, R is the ideal gas constant (8.314 J/mol·K), and T the absolute temperature in Kelvin. We have performed temperature dependent studies of the reaction rate constants in order to verify the Arrhenius behavior for the thermal reaction of the LOV domains and to correlate the pH effects to changes in the activation energies.

Kinetic measurements of adduct decay were performed within the temperature range from 20 to 30°C. For LOV1 at pH 7.8, the two time constants of the biexponential fit were evaluated separately. As shown in Figure 3.12A, the activation energy is 62 kJ/mol for the slow component of the decay whereas the fast component does not depend on the temperature within the experimental error. At acidic pH (pH 4.8) the activation energy rises to 78 kJ/mol as the dark form recovery slows down considerably. For LOV2, an Arrhenius plot of the decay rates yields an activation energy for each component of the biexponential decay which depends on pH (shown in Figure 3.12B). Again the activation barriers are higher at pH 4.9 with 65 and 100 kJ/mol for the fast and slow component, respectively, compared to 52 and 72 kJ/mol at pH 7.8. In LOV2, all contributions to the decay of the adduct are linearly dependent on the reciprocal temperature according to the Arrhenius equation. The activation energies at pH 7.8 are comparable to the 55 kJ/mol determined in LOV2 from *A. sativa* Phot1 [49]. In addition, through the investigation on LOV1-R58K mutant, it is found that the mutant does not influence the activation barrier for the adduct decay. The activation energy for the decay is 63 kJ/mol at pH 7.6, nearly the same as the value of the wild-type LOV1 at neutral pH.

In LOV1, the fast component of the adduct decay at pH 7.8 does not depend on the temperature. This implies that the underlying process does not have an activation barrier. As the slow component shows an activation energy of 62 kJ/mol, the two time constants might originate from two mechanistically different processes. Interestingly, the component without activation

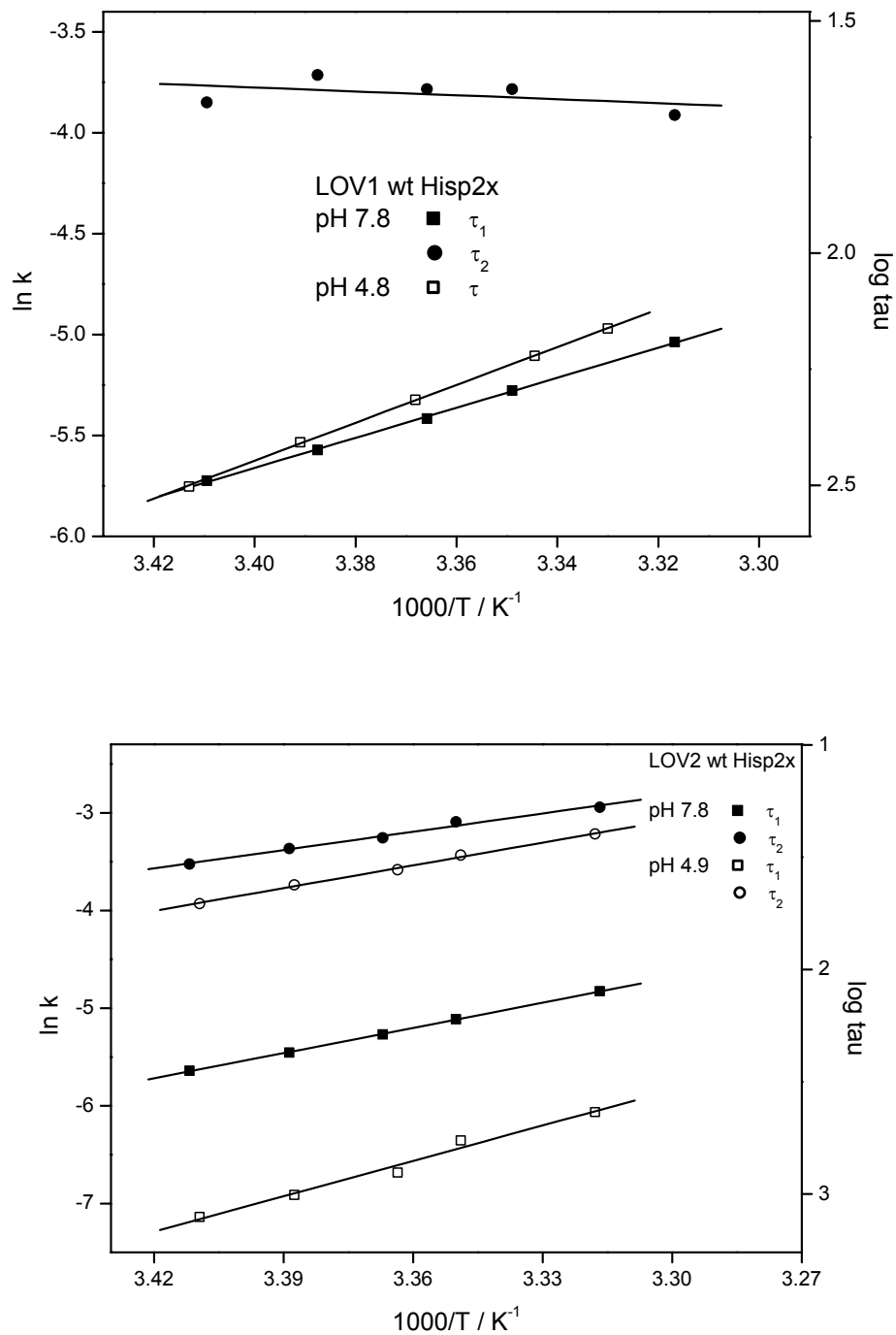


Figure 3.12. Arrhenius plot of the rate constants of the adduct decay. **A)** In the wild-type LOV1 domain. **B)** In the wild-type LOV2 domain. All the decay traces were fitted biexponentially except for LOV1 at acidic pH.

Results

energy disappears, when photo-inactive LOV2 is present in the LOV1+2-C250S mutant. In contrast, the components in LOV2 all show a considerable activation barrier with energy values of 52 to 100 kJ/mol. This point indicates another difference between two LOV domains. The linear dependence in the Arrhenius plots of LOV1 and LOV2 allows the conclusion that no heat capacity change is taking place during the conversion from LOV-390 to the dark form.

The same conclusion has been drawn from photoacoustic experiments [44]. This is in contrast to the last step in the photocycle of the photoreceptor photoactive yellow protein (PYP) [51]. In PYP the heat capacity change results from the exposure of hydrophobic sites to the medium [51]. Our findings support the hypothesis that no big conformational changes occur during the photocycle of LOV domains. Besides evidence from X-ray crystallography, where movements might be restricted, this has also been shown by FTIR difference spectroscopy in solution. There, the absence of strong amide difference bands rules out big conformational changes of the protein backbone in the LOV1 photocycle [52].

3.3.5 H/D Isotope Effect on the Thermal Backreaction

The standard LOV1 wild type sample was dialyzed into deuteriumoxid (D_2O , purity over 99.9%), under airtight condition. The proper quantity of solid $KHPO_4$, KH_2PO_4 and $NaCl$ were added in D_2O for keeping the pH value and ion concentrations at the same level as in the original sample, i.e. at pH ~ 8.0 and 10mM $NaCl$ and PO_4 . The UV-Vis absorption spectrum revealed no significant D_2O -induced structural change, but the decay time of the adduct increased by a factor of 3 compared to the value measured in H_2O . The observation of such a primary deuterium isotope effect indicates that the rate limiting step of the reaction involves breaking or formation of a bond involving a hydrogen atom that can be exchanged by D_2O [53].

Therefore, our observations indicate that formation or breakage of bonds involving hydrogen atoms and/or proton transfers are rate-limiting steps during the process of the adduct decay. This observation is in good agreement with a similar investigation on LOV2 from oat [49]. In this paper a large kinetic D/H exchange effect has been observed for the adduct decay in LOV2 wild type, however, only a very small effect on the triplet decay in the mutant LOV2-C39A (Arginine). The latter observation suggests that proton or hydrogen transfer is not the rate limiting step in the forward reaction leading to the adduct formation.

3.3.6 Photoreaction of the Mutant LOV1-C57G

To further clarify the adduct formation mechanism, the mutant LOV1-C57G was investigated. In the LOV1-C57G mutant, cysteine 57 of the wild type is exchanged against glycine. Because it lacks the reactive thiol group, no thiol adduct can be produced by blue light irradiation. However, after addition of a small amount of Ethanthiol ($\text{CH}_3\text{-CH}_2\text{-SH}$) into the sample containing LOV1-C57G, blue light irradiation generates a metastable species with absorption maxima at 570 and 615 nm (see Figure 3.13). The spectrum of the species resembles that of a typical neutral flavoprotein radical, FMNH^\cdot [33]. The species produced in this way reverts almost completely to the initial spectrum under dark condition, but much slower than ^3FMN . A similar attempt was also carried out with Mercaptoethanol ($\text{HO-CH}_2\text{-CH}_2\text{-SH}$). The result was similar but not as strong as with Ethanthiol, probably because Mercaptoethanol has lower polarity than Ethanthiol.

A very similar absorption band at 615 nm was previously observed when the LOV1-C57S mutant was irradiated in the presence of EDTA [32]. A somewhat different absorption band with maximum at 675 nm has been reported for the product of the photoreaction of yet another

mutant, LOV1-C57M, in which the reactive cysteine is replaced by methionine [32]. This species has been identified as a radical with a substituent attached to the N5 atom of FMN by electron paramagnetic resonance (EPR) studies [31].

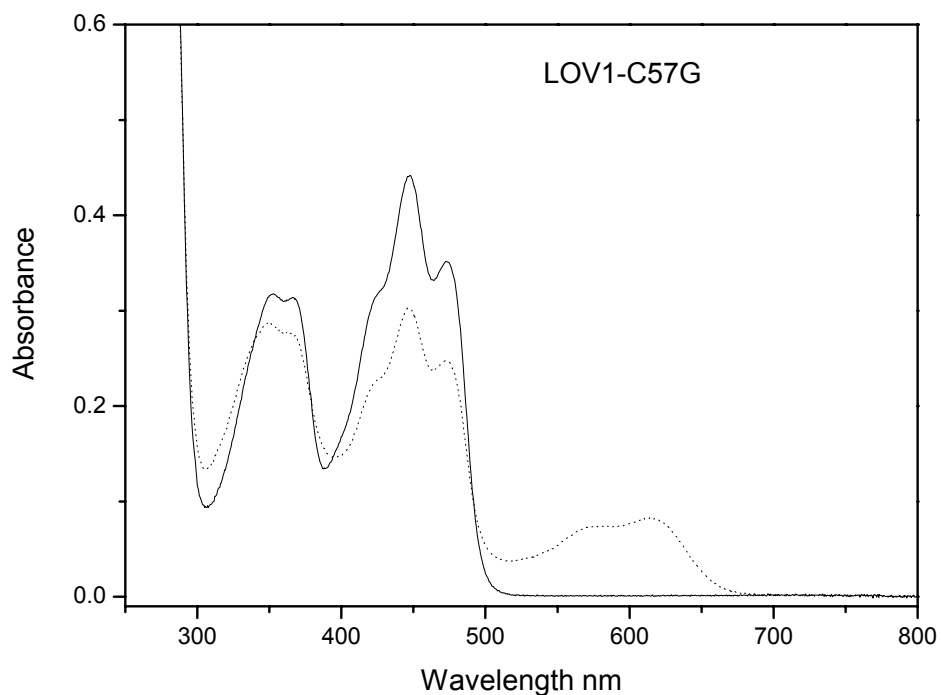


Figure 3.13. Irradiation of the LOV1-C57G mutant in the presence of ethanethiol. The solid line (—) shows the absorption spectrum of the sample before excitation by the strong light. The dotted line (.....) depicts the characteristic features at 570 and 615 nm of a flavoprotein neutral radical species generated by irradiation at 470 nm.

Hence the species generated in LOV1-C57G in the presence of thiol is assigned to the neutral radical FMNH^\cdot . This means that after excitation of FMN to the triplet state an electron is transferred from the thiol, followed by proton transfer to yield the neutral radical. However, no recombination of this radical with a thiyl radical occurs that would lead to a product similar to the adduct of FMN and cysteine. This might indicate that the thiol can come close enough to

the FMN for electron transfer, but can not enter the protein pocket close enough to form a bond with FMN.

In our work, the neutral radical could only be generated by fast irradiation with the powerful LED. The concentration of Ethanthiol and Mercaptoethanol added into the standard sample could not be determined very accurately because of their large volatility. This also prevented deoxygenation of the sample through bubbling with argon and a study under anaerobic condition.

3.3.7 Photochemical Back-reaction

The spontaneous back reaction from the adduct LOV-390 to the dark form LOV-447 is relatively slow compared with the formation process, so moderate blue-light irradiation should lead to a complete conversion into the adduct LOV-390. In the case of LOV1, however, it has been reported that the absorption band of FMN could not be bleached completely even with the highest light intensities available. This observation has been rationalized by the postulate of a photochemical backreaction. In order to test for the existence of such a reaction in the LOV2 domain, bleaching experiments were performed with various intensities of blue light from a 100 W tungsten lamp and UV light (280 ~ 390 nm) from a Xe lamp. The sample was illuminated with continuous light until the photostationary state was reached. The intensity of irradiation could be varied with different neutral density filters, and relative changes in absorbance $\Delta A/A_0$ at 475 nm were measured.

Whereas the tungsten lamp primarily excited the dark form, the UV light from the Xe lamp will excited dark form and adduct with similar probability. The alternative hypothesis of a photoinactive fraction of FMN should be tested. In the presence of a photochemical

Results

backreaction this should lead to different photostationary states. In order to obtain the limit of bleaching of the absorption, a high power light source (1-W blue LED) was used to irradiate the sample at 470 nm for 1 s. The results are collected in Figure 3.14. The absorption spectra of both species are also shown in comparison to the transmission spectrum of the filter combination used for UV irradiation and the emission spectrum of the blue LED.

In the case of the LOV1 domain the following model of a photochemical backreaction has been proposed: the dark form (species 1) is photochemically converted to the adduct (species 2) with an apparent rate constant $F\alpha_1$ given by

$$F\alpha_1 = F\Phi_1 \int \varepsilon_1(\lambda)\rho(\lambda)d\lambda \quad (3.12)$$

in this expression, F is the total photon flux, Φ_1 the quantum yield of decay to the intermediate, $\varepsilon_1(\lambda)$ the extinction coefficient of species 1, and $\rho(\lambda)$ the normalized quantum emission spectrum of the light source. The back reaction can occur either thermally with rate constant k_2 , or photochemically with an apparent rate constant $F\alpha_2$ defined in analogy to that of the forward reaction. In the photostationary state the concentration c_j of both species are related by

$$x_s = \frac{c_2}{c_1 + c_2} = \frac{\alpha_1 F}{k_2 + (\alpha_1 + \alpha_2)F} \quad (3.13)$$

Where x_s is the mole fraction of the photoreactive FMN that is in the adduct state. The absorbance (A_F) of this sample measured at a probe wavelength λ' is expressed in terms of this relative population by

$$A_F(\lambda') = c_0 x_s \varepsilon_2(\lambda') + c_0 (1 - x_s + x_i) \varepsilon_1(\lambda') \quad (3.14)$$

Where c_0 is the total concentration, i.e. the concentration of the dark form before irradiation.

Results

When A_0 is the absorbance of the sample without photolytic irradiation, the relative bleaching induced by the light of intensity F is given by

$$\frac{\Delta A}{A_0} = \frac{A_0(\lambda') - A_F(\lambda')}{A_0(\lambda')} = \frac{\varepsilon_1(\lambda') - \varepsilon_2(\lambda')}{(1 + x_i) \varepsilon_1(\lambda')} \frac{\alpha_1 F}{k_2 + (\alpha_1 + \alpha_2) F} \quad (3.15)$$

Hence a plot of $\Delta A/A_0$ vs. F should be fitted by the expression

$$\frac{\Delta A}{A_0} = \frac{RF}{\alpha + F} \quad (3.16)$$

Where the parameters R and α have the interpretation

$$\alpha = \frac{k_2}{\alpha_1 + \alpha_2} \quad (3.17)$$

$$R = \lim_{F \rightarrow \infty} \left\{ \frac{\Delta A(\lambda')}{A_0(\lambda')} \right\} = x_a \frac{1 - \varepsilon_2 / \varepsilon_1}{1 + \alpha_2 / \alpha_1} \quad (3.18)$$

where $x_a = I/(I+x_i)$ is the mole fraction of photochemically active FMN. R is the saturated value at infinite intensity, and α is the intensity at which half of the saturation is obtained. Because both ε and α are positive quantities, the value of R is bound by $R \leq 1$. The upper limit $R = 1$ is obtained when both the photoadduct has no absorption ($\varepsilon_2 = 0$) and the photochemical back reaction does not occur ($\alpha_2 = 0$). On the other hand, $R < 1$, the value can provide ranges for ε_2 or α_2 as

$$0 \leq \frac{\varepsilon_2}{\varepsilon_1} \leq 1 - R, \quad 0 \leq \frac{\alpha_2}{\alpha_1} \leq \frac{1}{R} - 1 \quad (3.19)$$

Whereas this function provided a very good fit with the data for LOV1, the corresponding fit to the data for LOV2 shown as the dotted line in Figure 3.14 is rather poor. This is attributed to

Results

the fact that in LOV2 two species with distinctly different decay rate constants coexist with sizeable concentration. Hence the fitting function should be extended to

$$\frac{\Delta A}{A_0} = \frac{R_f F}{\alpha_f + F} + \frac{R_s F}{\alpha_s + F} \quad (3.20)$$

Where the subscripts f and s refer to the fast and slowly decaying components, respectively. The fit with this function is shown as the full line in Figure 3.14B. In order to reduce the number of independent parameters for the fit, the ratios $\alpha_f / \alpha_s = 9$ and $R_f / R_s = 1/3$ have been fixed to the values corresponding to the rate constants and amplitudes observed from the decay kinetics (Table 3.2). This encloses the additional assumption that the quantum yields are the same for the fast and the slow component. The extrapolated limit for bleaching with blue light are $R = 0.882 \pm 0.003$ for LOV1 and $R_f + R_s = 0.91 \pm 0.006$ for LOV2, which indicates that about 9 ~ 12% of the absorption at 475 nm cannot be bleached. It is seen from the picture that the spectrum of this light source has little overlap with the spectrum of the adduct. If we assume that under these conditions the adduct is not excited and no photochemical backreaction can occur, the value $R_f + R_s$ leads to the estimate $\varepsilon_2 / \varepsilon_1 \sim 0.09$ for the ratio of the extinction coefficients. When bleaching is performed with UV light from a Xe lamp that excites both the dark form and the adduct with similar probability, the photostationary state contains slightly more (3%) of the dark form. This might imply a small value for the ratio of the photochemical reaction coefficients of $\alpha_2 / \alpha_1 \approx 0.05 \sim 0.09$. Hence it is possible thought not very likely that there is a photoinduced reaction from LOV2-390 back to LOV2-447. This is consistent with the finding in literature that even at high-intensity light excitation at 428 nm a fraction of about 7% of the non-covalently bound FMN remains non-converted to an FMN-Cysteinyll adduct because of photo-induced back-relaxation of the adduct to non-covalently bound FMN [46, 54].

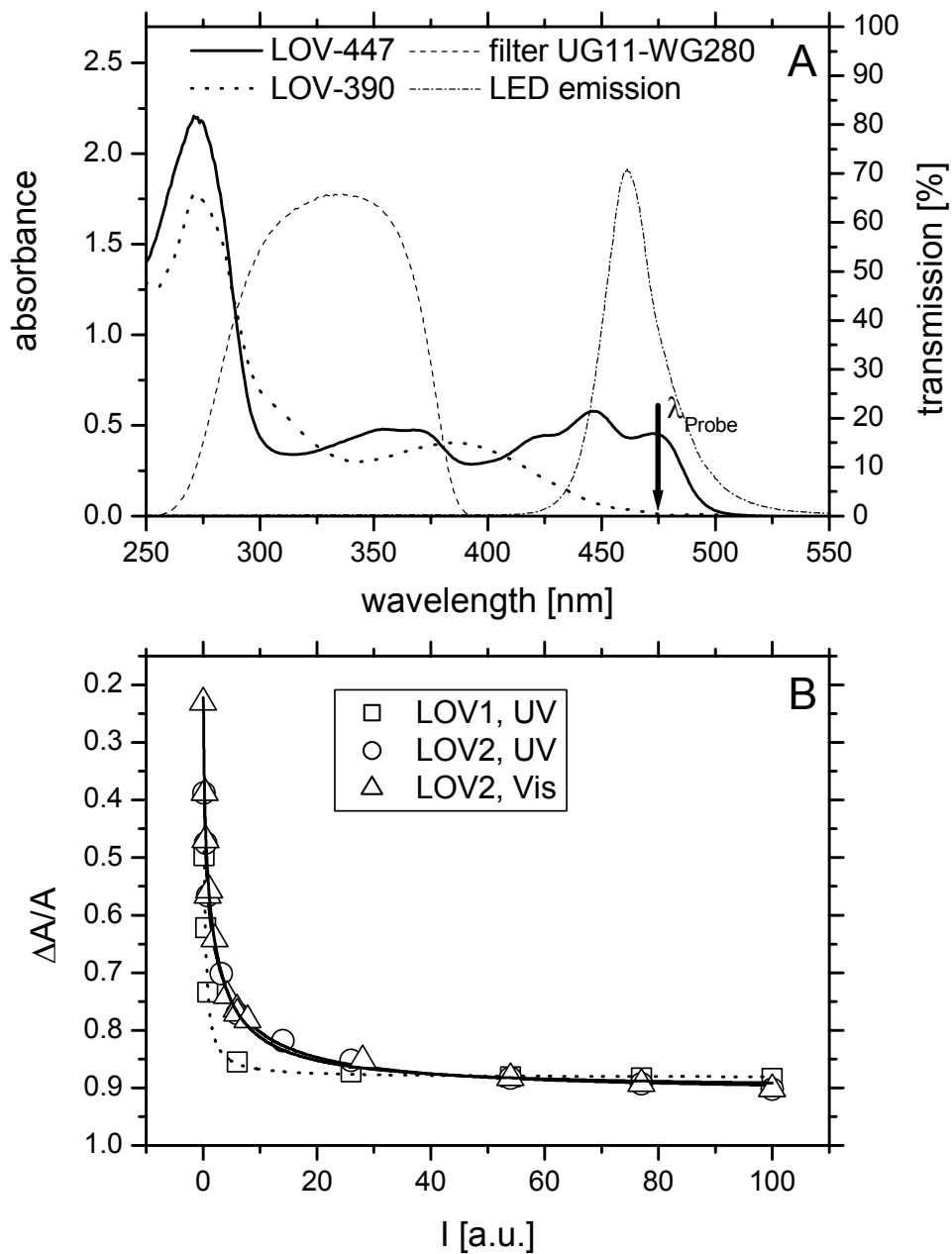


Figure 3.14. (A) Absorption spectra of the dark form and the adduct in relation to the transmission spectrum of the filter combination used for UV irradiation and the emission spectrum of the blue LED. (B) Bleaching $\Delta A/A$ of the absorption at 475 nm under the influence of blue light from a tungsten lamp (LOV2, triangles) and UV light in the range 280 ~ 390 nm (LOV1, squares and LOV2, circles).

Results

However, the similarity of the results for irradiation with blue light and UV light could equally well be explained by the assumption that a small fraction of FMN in the protein cannot undergo the photoreaction to form the adduct state for reasons that are not yet understood.

In order to compare LOV2 domain with LOV1 directly, the LOV1 was reinvestigated under the same conditions. In order to establish the limit for bleaching of each LOV domain, very strong bleaching with a high power (1 Watt) blue LED at 470 nm for 1 s was applied and resulted in $\Delta A/A = 0.91$ for LOV1 and $\Delta A/A = 0.93$ for LOV2. This indicates that about 7 ~ 9 % of the absorption at 475 nm cannot be bleached, and suggests that the bleaching does not extrapolate to 100% even at infinite light intensity of a light source which has little spectral overlap with the adduct state spectrum. We estimate that the absorption coefficient of the adduct at 475 nm is less than 4% of that of the dark form. Since the spectrum of the LED has little overlap with the spectrum of the adduct, we may set $\alpha_2/\alpha_1 \approx 0$ and obtain $x_a = 0.948$ for LOV1 and $x_a = 0.969$ for LOV2. Hence about 3 ~ 5 % of the FMN in the sample cannot be converted to the adduct by the strong LED light pulse, whereas 5 ~ 8 % is not converted by UV light of infinite intensity that excites both the dark form and the adduct with similar probability. The ratio of the two bleaching limits for UV and LED irradiation is, according to our model, given by

$$\frac{R_{LED}}{R_{UV}} = \frac{1 + (\alpha_2 / \alpha_1)_{UV}}{1 + (\alpha_2 / \alpha_1)_{LED}} \quad (3.21)$$

If a photoreaction induced by the LED can be neglected, this leads to $\alpha_2 / \alpha_1 \approx 0.034$ for LOV1 and $\alpha_2 / \alpha_1 \approx 0.022$ for LOV2 for UV irradiation. If the overlap of the spectrum of the LED with that of the adduct is sufficient to induce some backreaction, these numbers could even become slightly larger. Hence there is some evidence for a photochemical backreaction, albeit with a much smaller quantum yield as compared to the forward reaction.

4 The Photocycle of LOV2

Any model for the photocycle in LOV domains must account for the lack of reactivity in the dark and the light-activated formation of a transient covalent adduct between the catalytic cysteine and C (4a) on the isoalloxazine ring.

The results of the investigation on the LOV2 domain can be summarized into the picture of the photocycle presented in Figure 4.1. Following photoexcitation to the FMN first singlet excited state, the LOV2 dark form converts to the triplet state through intersystem crossing (ISC). The triplet could be observed in transient absorption spectroscopy as species LOV2-715. In the LOV2-C250S mutant, this triplet state LOV2-715 cannot proceed to the LOV2-390 intermediate because it lacks the reactive thiol group, then it returns to the ground state LOV2-446 with a main time constant of $\sim 290 \mu\text{s}$ and a minor time constant of $\sim 12 \mu\text{s}$, which indicates the presence of two subspecies exhibiting identical spectra. But the minor subspecies disappears after removal of oxygen. In the wild type, the decay of this triplet is very fast and exhibits single-exponential with a time constant of 500 ns under formation of the adduct state LOV2-390.

The backreaction of LOV2-390 to LOV2-446 in the dark is double exponential in the whole pH range investigated (4.8 \sim 10.0). Hence, two species are involved which can, however, not be distinguished on the triplet level or in their dark forms. They also share identical spectra and decay back to the dark state LOV2-446 independently. The situation of these two adduct

The Photocycle of LOV2

species is quite different from that in LOV1, where a minor fast component in the decay of the adduct is only discernible at high pH value (pH > 7.5). Moreover, the decay times in LOV2-390 are not affected by chloride, in strong contrast to the behavior of LOV1-390.

Compared to the photocycle of LOV1 [30], the process in the LOV2 domain appears to be a little bit more complicated. In the LOV2 domain, the lifetime of the triplet state is very short (500 ns) in the wild type, but extremely long in the mutant LOV2-C250S. The corresponding data in LOV1, are 800ns and 4 μ s for two species in the wild type, and 27 μ s for the mutant LOV1-C57S.

The presence of two LOV domains in Photoreceptor from *C. reinhardtii* naturally poses the questions about the relation between these two domains. How does one domain interact with the other in the dark state, and how does this interaction change in the signal state? Photoactivation of each domain might have the same effect in the biological response, but a cooperative or counteroperative effect could also be conceived. The investigation on the double domains (LOV1+2-wt, LOV1+2-C57S, LOV1+2-C250S), lead to the conclusion that the triplet states apparently do not interact, but decay with the time constants of the corresponding single domains. The rates of the thermal back-reaction from the adduct to the ground state do, however, depend on the presence of a second domain. The single isolated LOV domains show a second component in the decay, which disappears upon interaction with the other domain in the double domain constructs. Furthermore, the pH dependence of the LOV2 adduct decay is not present anymore in the LOV1+2-C57S mutant, which might be caused by a coverage of the protonation site. Interestingly, calmodulin-binding proteins seem to have a similar effect on the single LOV domains. Hence, one might speculate that the species leading to the second decay time in the kinetics of the single domains are in fact dimers.

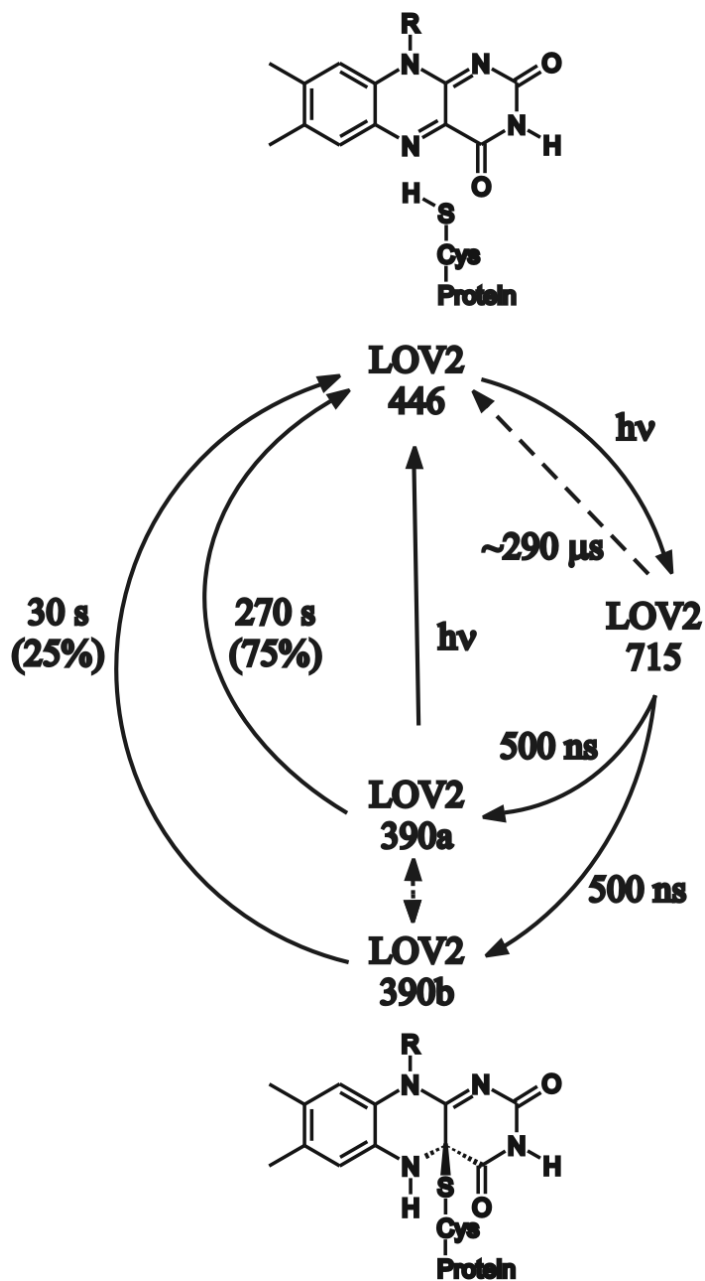


Figure 4.1. Photocycle of the single wild-type LOV2 domain from *C. reinhardtii* Phot

5 Comparison of Models for the Photocycle

5.1 Global fit procedure

Blue light irradiation of the LOV domains from *C. reinhardtii* Phot produces a cysteinyl adduct at the flavin C(4a) position, which decays back to the dark state thermally. To elucidate the information during this process, we investigated the kinetics of the formation and the decay of the long-lived intermediate. From the analysis on the sequence of the LOV domains' absorption spectra after irradiation, only one absorption peak was seen in the spectrum of the intermediate. Target factor analysis [55] of the absorption spectra of LOV domains after strong illumination clearly indicate that all spectra can be described as the superposition of only two components. The fact that a biexponential function is needed for the modeling of the time traces indicates, on the other hand, that at least three species must be involved. Hence two or more dark forms might exist which have indistinguishable absorption spectra. Alternatively, or in addition, several adduct species with identical absorption spectra might exist.

It is obvious that the analysis of a single decay event cannot yield sufficient information that would permit a distinction between these different models. Hence two sets of experiments were performed with each domain in which the system was excited with light of different intensity and the decay followed for ca. 1000 s. Although the absolute light intensity could not be measured, the relative excitation rate for the different bleaching experiments was determined precisely. In one set of experiments, in the following referred to as “fast” bleaching

Comparison of Models for the Photocycle

measurements, excitation was performed with two high-intensity LEDs which produce a light beam of 1 W of light at 460 nm. These LEDs were mounted opposite to each other with a spacing of 1 cm to allow the insertion of a standard quartz cuvette. The light fluence was controlled by setting the duration of the current pulse applied to the LEDs in the range 25 ~ 500 ms. This time is much shorter than the rate constants of ground state recovery under investigation (20 ~ 800 s). The setup was calibrated by measuring the duration of the light pulse as a function of the current pulse duration with a photodiode. In the second set of experiments called the “slow” bleaching measurements the sample was irradiated for 1000 s by the light of a tungsten lamp. This time is long compared to the thermal recovery times and allows for several excitation cycles of the same molecule. Hence accumulation of a light-adapted form should be possible in this experimental configuration in contrast to the “fast” bleaching scheme. With slow bleaching, different excitation intensities were set by neutral density filters. An additional GG430 filter was used to cut off light with wavelengths shorter than 435 nm to avoid excitation of the photoproduct. The transmission curves of these filter combinations are shown in Figure 5.1A, the spectrum of the longest wavelength band of FMN in the dark forms of the LOV domains and the product of the filter curves with the absorption spectrum. The area under these curves corresponds to the effective excitation intensity of the sample when constant spectral intensity of the lamp and constant quantum yield is assumed in this spectral range. The transmission of the sample at 475 nm was observed during slow bleaching and during the recovery in the dark after each excitation cycle. At this wavelength only the dark states contribute to the absorption. In order to reduce some avoidable error disturbing the result, the pH, the volume and the concentration of the samples were prepared to be nearly the same level for fast and slow bleaching experiments. Also, temperature and the path length were always kept identical.

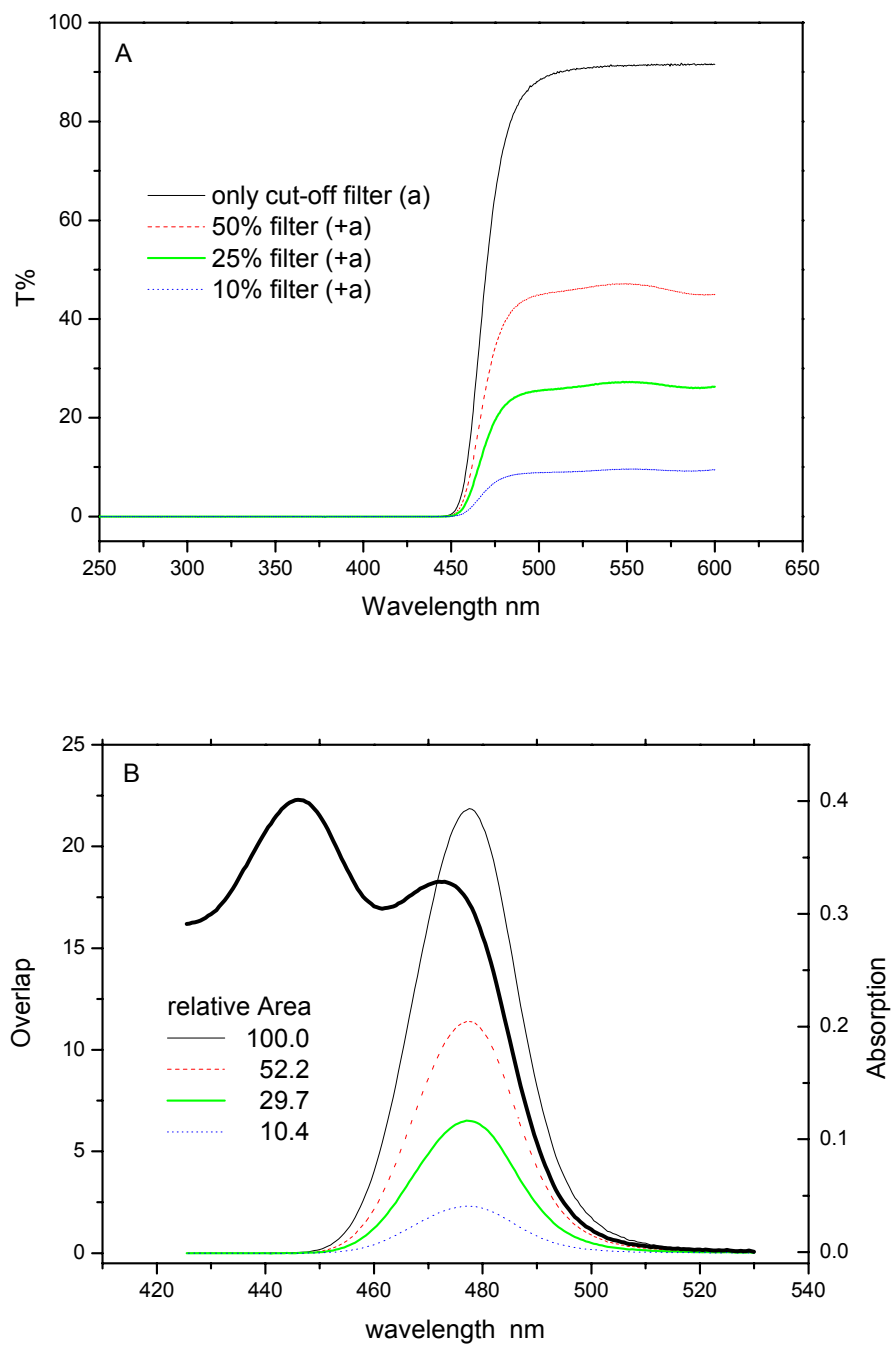


Figure 5.1. A) Transmission spectra of the filter combinations used to modify the light intensity in the “slow” bleaching experiments. B) Absorption spectrum of the longest wavelength band of FMN in the dark form of the LOV domains and the product of the filter curves with the absorption spectrum.

Comparison of Models for the Photocycle

The bleaching and recovery curves obtained for the LOV1-p2X domain at pH = 8 are shown as an example of the experimental data sets in Figure 5.2. Each of these curves can be fit reasonably well by a biexponential function. However, the rate constants obtained in this way vary considerable from curve to curve. On the other side, all models that involve only unimolecular excitation and decay steps lead to decay rate constants in the dark that are independent of the excitation history of the sample. Only the relative amplitudes of the two decay components may change. Furthermore, the relative amplitudes of the decay components should depend on the intensity and duration of the excitation in a well defined way, depending on the model chosen. Hence these parameters should not be considered independent for each kinetic curve. Rather, all experimental curves should be fitted simultaneously to the same set of variables with all other known parameters of the particular model (e.g. the relative excitation intensities and durations) fixed. For this purpose a computer program was developed which can perform a “global fit” of several data sets to several functions controlled by a common set of variables and parameters.

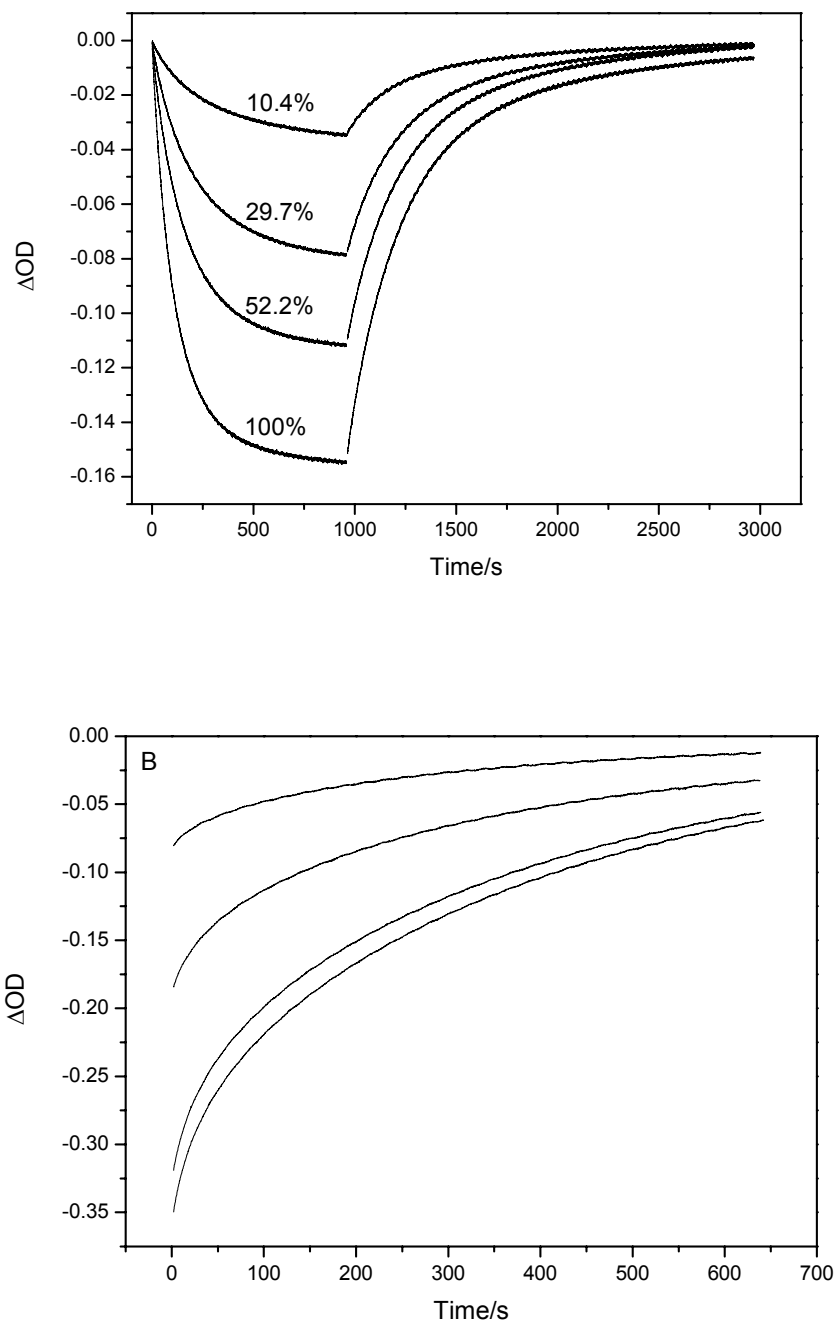
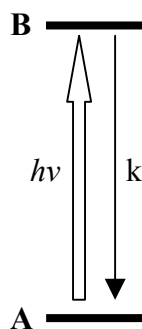


Figure 5.2. The data set obtained for slow bleaching and recovery after slow bleaching (A) and for recovery after fast bleaching (B) of LOV1 at pH = 8

5.2 Models

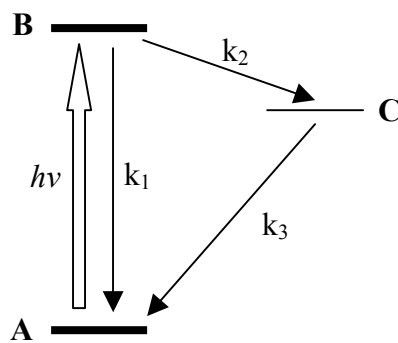
In the photocycle of LOV domains, the cysteinyl adduct decays spontaneously back to the ground state in the dark after the photoproduct formation. We have constructed several models, which could explain the photoreaction processes in the photocycle of LOV domains, especially the process of the formation and decay of the adduct. The kinetics parameters, such as relative quantum efficiencies and rate constants, might help us to understand the mechanism of photoreactions in the photocycle and the possible interaction between two domains. In the following seven models are presented according to their increasing complexity.

Model I:



This model considers only two levels, where A is the ground state and B is the excited state. k is the rate constant of the thermal decay of the excited state to the ground state. This is the most simple model for portraying a photocycle. But from the experimental data, for the wild-type samples at high pH ($\text{pH} \geq 7.5$), there are at least two time constants obtained by fitting the recovery traces exponentially. Hence this simplest model cannot be matched with this phenomenon. One option is to assume an intermediate C resulting in the new model II.

Model II:



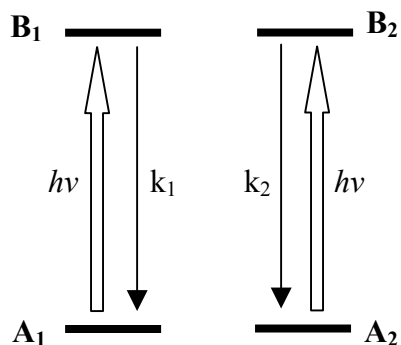
There are 3 levels in this model. The ground state A, the excited state B and the metastable intermediate C. A is excited into B under irradiation, and B crosses into C, then C reverts to the ground state A in dark condition. Two options might be considered for state C: Either it has the same absorption spectrum as the adduct, or it is a species which has no significant absorption in the range 300 ~ 500 nm. For the present purpose of the fit to the absorption recovery at 475 nm both options have identical consequences and can hence not be distinguished. Three reaction rate constants enter into this model. The solution of the corresponding differential equation yields a double exponential recovery of the ground state A. Hence this model could be compatible with our experimental data. However, the alternative model III presented below also predicts a biexponential recovery of the ground state absorption.

Model III:

In this model, both the ground state and the excited state are considered to exist in two conformations, A_1 and A_2 , B_1 and B_2 , respectively. Under light irradiation, the excited states come into being from the dark form: $A_1 \rightarrow B_1$, $A_2 \rightarrow B_2$. However, they are two independent

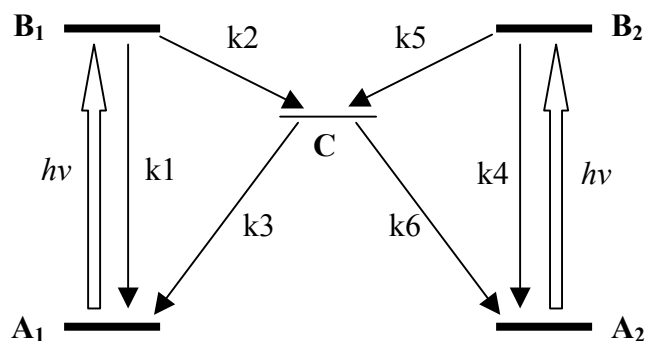
Comparison of Models for the Photocycle

systems like model 1. Easily seen from the scheme of this model, there are two rate constants but without direct connections between the two photoreactive processes. Models II and III both predict a double exponential recovery of absorption, however the amplitudes of the two components will depend differently on the intensity used for bleaching.



As will be discussed in the following, the fit based on model III is not satisfactory. Model III could be extended by the assumption of a thermal reaction between the two dark forms. However, we found that this extension did not improve the fit.

Model IV:



In this model, an intermediate C is added like in model III which connects the two ground states. When the ground states A_1 and A_2 are excited into the excited states B_1 and B_2 by photoexcitation, both B_1 and B_2 are transferred into the metastable species C. Then C decays

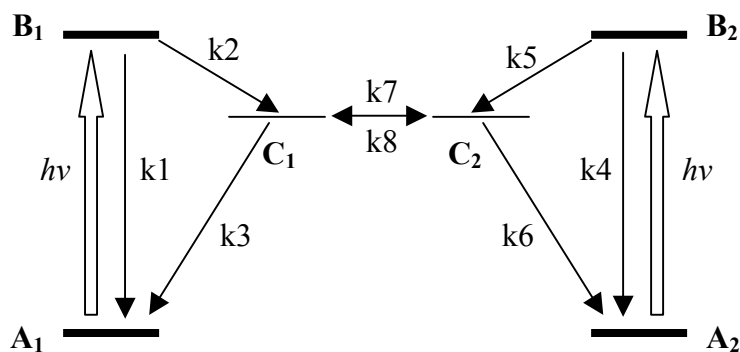
Comparison of Models for the Photocycle

back to the ground states A_1 and A_2 at the same time in the dark. This model can account for light-adaptation of the system. E.g., in the dark adapted state only species A_1 might exist, whereas after prolonged excitation species A_2 will accumulate. Hence such a model can explain different decay rate constants in the slow and fast bleaching experiments.

Model V:

Model IV will allow for a change in the relative amounts of the two dark species during irradiation, but will not allow recovery to the dark adapted state. If the latter process occurs on a time scale comparable to the adduct decay, a thermal reaction between the two ground states must be allowed for as well. Hence, two more rate constants increase the complexity of this model. For the reason of its high similarity to Model IV, the schematic diagram of Model V was not pictured here.

Model VI:



This model considers 6 levels. It is derived from model IV, There are now two intermediates of the type C, produced from B_1 and B_2 , respectively, which can thermally interconvert. If this

exchange is slow enough, the recovery rates from the intermediates to the two ground states can be different.

Model VII:

This is the most general model for the 6 levels case studied here. It allows for thermal equilibrium between the two dark states A_1 and A_2 as well as the adduct forms, C_1 and C_2 , like in model VI. Hence two more rate constants should be added in this complicated model compared to Model VI. Altogether, there are 10 rate constants that need to be taken into account in the process of the whole photocycle. Its schematic diagram was not pictured here.

In principle, no matter whether excitation is done by fast or slow bleaching, the regeneration process of the adduct in the same domain should display the same rate constants in the dark (albeit with amplitudes that depend on the excitation history), if some influence factors are kept the same, like pH, concentration of FMN, temperature, and the light pathway. Hence, these conditions were well controlled during the whole procedure of measurements. For slow bleaching the time behavior of the absorption could also be followed during the bleaching. This is not possible in the case of fast bleaching, since the absorption spectrometer can take data only in 0.2 s intervals. The data set for each global fit consists of twelve kinetic traces, namely four slow bleaching traces and eight recovery traces.

5.3 Analysis of data for LOV1

Firstly, the LOV1 wild-type (His-p2X) was investigated under standard conditions. Because the process of the bleaching and recovery in LOV1 appears to be much simpler at acidic condition

Comparison of Models for the Photocycle

than at neutral pH, the wild-type LOV1 was also explored at pH 4.8. Under these conditions the simplest model I resulted in a reasonable fit, shown in Figure 5.3. At neutral pH, the complexity of the model had to be increased up to model VII for an acceptable fit (see Figure 5.4). In both figures, graph A is for the slow bleaching measurements, including both bleaching and recovery curves, and B is for the fast bleaching measurements. The optimized values of the model parameters are given in Table 5.1.

Table 5.1. Rate constant values obtained by fitting with reasonable models

LOV1 at pH 8		LOV1 at pH 4.8	
Rate constant		Rate constant	
k_{B1-A1}	0.23e-01	k_{B-A}	0.27e-02
k_{B1-C1}	0.21e-01	-	-
k_{C1-A1}	0.38e-03	-	-
k_{B2-A2}	0.17e+01	-	-
k_{B2-C2}	0.14e+00	-	-
k_{C2-A2}	0.39e-02	-	-
k_{C1-C2}	0.27e-03	-	-
k_{C2-C1}	0.87e-03	-	-
k_{A1-A2}	0.83e-06	-	-
k_{A2-A1}	0.55e-07	-	-

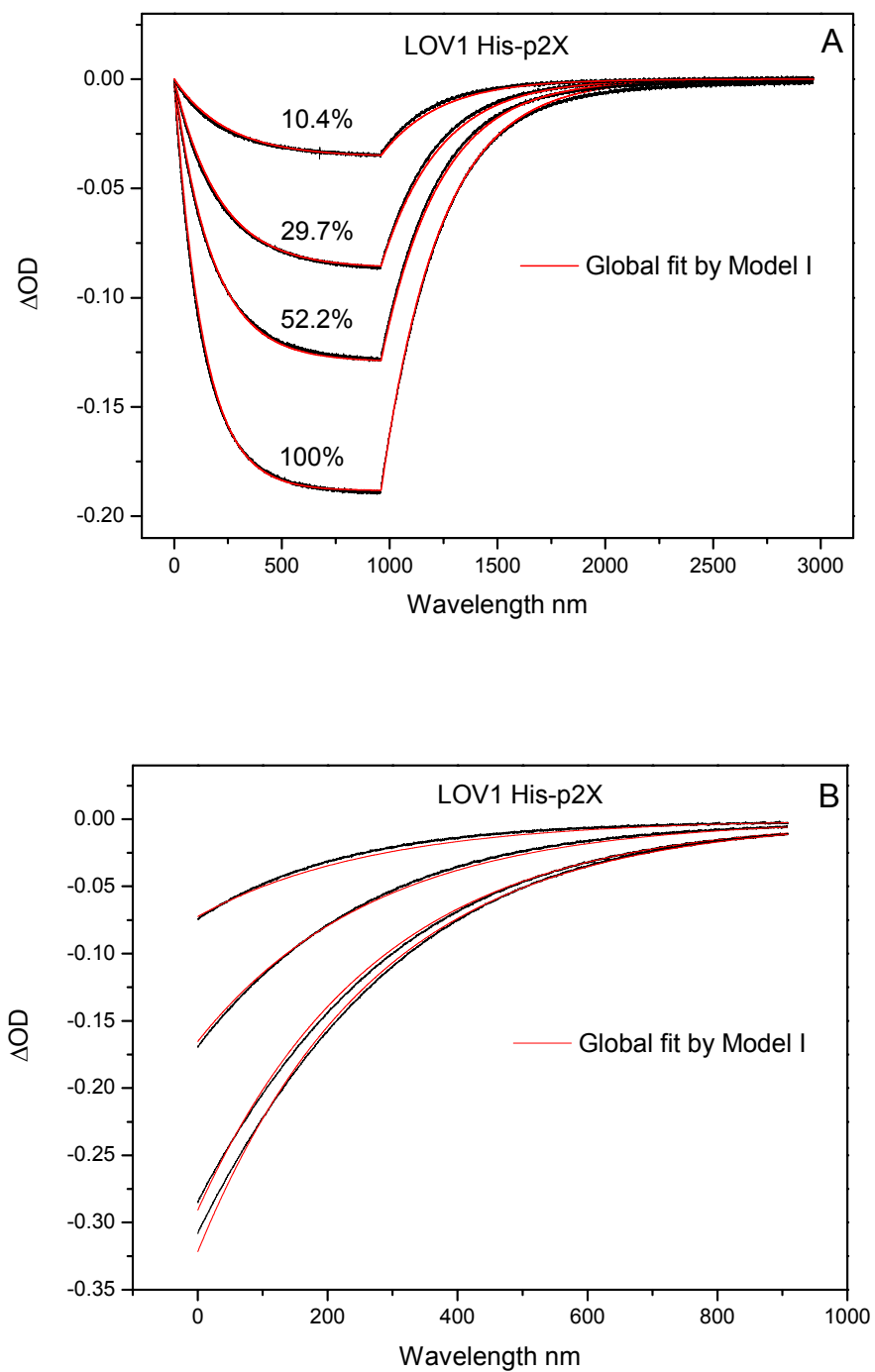


Figure 5.3. Global fit by model I of the data set of LOV1 at pH 4.8

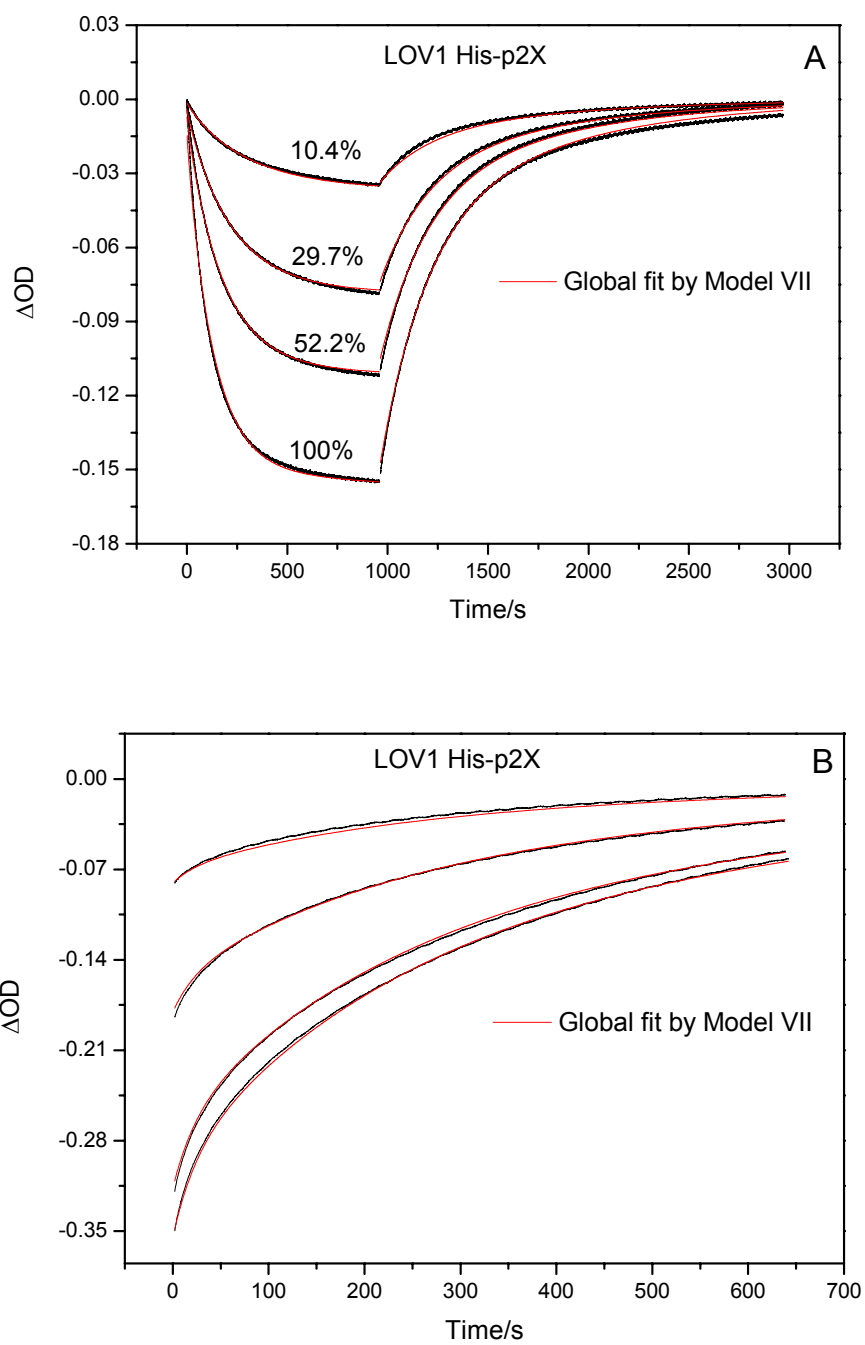


Figure 5.4. Global fit by model VII of the data set of LOV1 at pH 8

5.4 Analysis of data for LOV2

In contrast to LOV1, the LOV2 domain exhibits a complicated decay behavior at all pH values. Hence only the standard sample at neutral pH was examined in the global fit. As in the case of LOV1, a model of the complexity of model VII is required for an acceptable fit. For the reason of quite similarity to the fit of LOV1 at pH 8, the fit curves were not shown here. All of the rate constant values obtained by global fit with model VII were listed in Table 5.2. In comparison to the result obtained for LOV1, the rate constants connecting the two dark states are rather small in both single domains.

Table 5.2. Rate constant values of LOV2 His-p2X obtained by fitting with model VII

Rate constant		Rate constant	
k_{B1-A1}	0.30e-01	k_{B2-A2}	0.12e+01
k_{B1-C1}	0.46e-03	k_{B2-C2}	0.36e+00
k_{C1-A1}	0.37e-07	k_{C2-A2}	0.41e-02
k_{C1-C2}	0.59e-03	k_{C2-C1}	0.29e-02
k_{A1-A2}	0.66e-05	k_{A2-A1}	0.24e-05

The X-ray structure of the LOV1 domain shows that the protein is present in two conformations that differ in the orientation of the cysteinyl SH group relative to the FMN chromophore [28]. Quantum chemical calculation show that the two conformations are stabilized by different interactions of the hydrogen atoms in cysteine with the flavin N(10) nitrogen. Electronic excitation does not seem to influence the interactions in either conformation. However, since only movement of a SH-group is required, interconversion between these conformers should be much faster than the timescale of the dark state recovery. Also, the X-ray structure of other

LOV domains does not show two conformers, and for LOV2 of *C. reinhardtii* the X-ray structure is not known. Hence it is more likely that the two dark state species suggested by the model VII fit are two conformers of the protein that require larger and complex movements for interconversion. Such interconversions could indeed last very long [56].

5.5 Analysis of data for LOV1+2

In the double domain LOV1+2, two LOV domains can perform the photocycle. Hence a rather complicated kinetic of the ground state recovery was expected. However, the two mutated double domains LOV1+2-C57S and LOV1+2-C250S each show only a single decay time. The mutant LOV1+2-C57S shows only the fast component of adduct decay and LOV1+2-C250S shows only the slow component. This is in contrast to the individual domains LOV1 and LOV2. Apparently, the existence of a second inactivated domain attached to a single active LOV domain suppresses one of the two decay channels present in an isolated LOV domain. This clearly indicates some interdomain interaction which blocks one pathway of the adduct decay observed in the isolated wild-type part. Comparison of two mixed-domain S-mutants suggests that inactivated LOV1 has a stronger effect on LOV2 than inactivated LOV2 on LOV1. In the global fit, both mutated double domains LOV1+2-C57S and LOV1+2-C250S were examined at neutral pH, and model II could fit those time traces quite well. The global fit by model II of the time traces of LOV1+2-C250S was pictured in Figure 5.5. That of LOV1+2-C57S was not shown here. Table 5.3 lists the rate constants of both mix-domains.

The wild type double domain LOV1+2 shows again a double exponential decay, which requires a fit by a more complicated model.

Table 5.3. Rate constant values of the double mix-domains obtained by fitting with model II

LOV1+2-C250S		LOV1+2-C57S	
Rate constant		Rate constant	
k_{B-A}	0.31e-02	k_{B-A}	0.41e-01
k_{B-C}	0.71e-03	k_{B-C}	0.32e-01
k_{C-A}	0.16e-02	k_{C-A}	0.28e-01

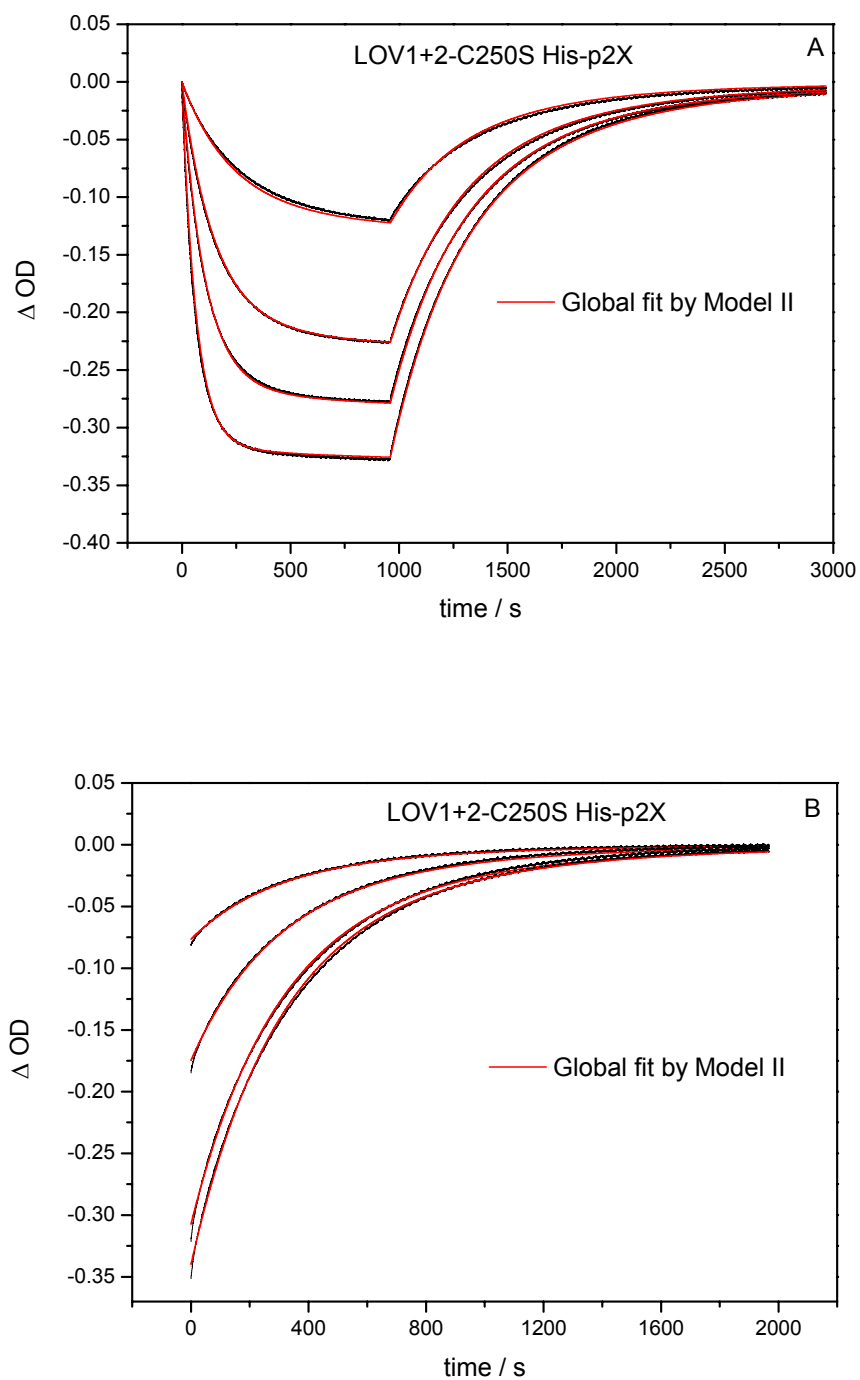


Figure 5.5. Global fit by model II of the data set of LOV1+2-C250S at pH 8

6 Mechanism of the formation of the adduct

6.1 Possible photoreaction scheme of the adduct formation

The photochemical reactions observed for the LOV1 and LOV2 domains of phototropin suggest that the reaction mechanism involves the formation of a similar flavin-thiol adduct. Formation of the flavin-thiol adduct requires the presence of at least one cysteine in proximity to the flavin chromophore. Both LOV domains contain a conserved cysteine residue, which plays a crucial role in the formation of the postulated light-induced flavin-cysteinyl adduct, with the protein bound FMN chromophore.

In the LOV1 domain Cys57 is the reactive position for the formation of a cysteinyl adduct and it is Cys250 in LOV2. Mutations at these two positions in LOV domains were introduced for understanding the importance of cysteine near the FMN chromophore. These can be evidenced through the investigation of LOV1-C57S and LOV2-C250S, in which the reactive cysteine is replaced by a nonreactive amino acid, serine. In these mutants, the formation of the adduct is not possible due to the absence of a thiol group. Alternatively, the key reactive cysteine can also be displaced by another nonactive amino acid without -SH group, like alanine, glycine etc. It was observed that illumination with blue-light did not affect the absorption of these mutants, and no light mediated photobleaching was detected. However, these mutants are competent in the early photochemical steps, the formation of the triplet state.

Mechanism of the formation of the adduct

All LOV domains demonstrate a similar photocycle, which should be governed by the same general reaction mechanism. This photocycle can proceed limitless times if the environment around the chromophore FMN is not destroyed. Some progress has been made in the understanding of the overall photoreaction. A flavin C(4a)-thiol adduct is produced via the FMN triplet excited state, ^3FMN , after illumination by blue light and then this adduct thermally reverts to the dark form. However, the mechanistic and conformational steps of the photocycle, how the photoadduct, LOV-390, is formed from the triplet state, have not been conclusively established. A clear deuterium isotope effect has indicated that the step of formation or breakage of bonds involving hydrogen atoms is rate limiting only in the thermal backreaction. Several mechanisms for the adduct formation can be conceived. Three hypotheses are presented and discussed below.

6.1.1 Ionic Model

One widely proposed pathway is ionic transfer mechanism [23]. The cysteine residual is initially present as a thiolate. The triplet excited state of FMN, ^3FMN is protonated at N(5) by a proton-donating group nearby in the protein to give the FMNH^+ cation. The FMNH^+ carbocation, which formally has a positive charge at C(4a), is the electrophile that could form a bond with the nucleophilic thiolate, and then the adduct could be generated. The schematic graph is shown in Figure 6.1. In this mechanism, obviously, the thiolate and FMNH^+ cation should be present before the adduct formation occurs. However, it has been demonstrated that in solution the flavin triplet protonation occurs only at $\text{pH} < 4.4$, and ^3FMN follows electron transfer by protonation to form a neutral flavin radical at pH range $4.4 \sim 8.3$ [57]. These

Mechanism of the formation of the adduct

observations contradict the ionic mechanism. It is hence unlikely to explain the process of photoreaction under standard conditions.

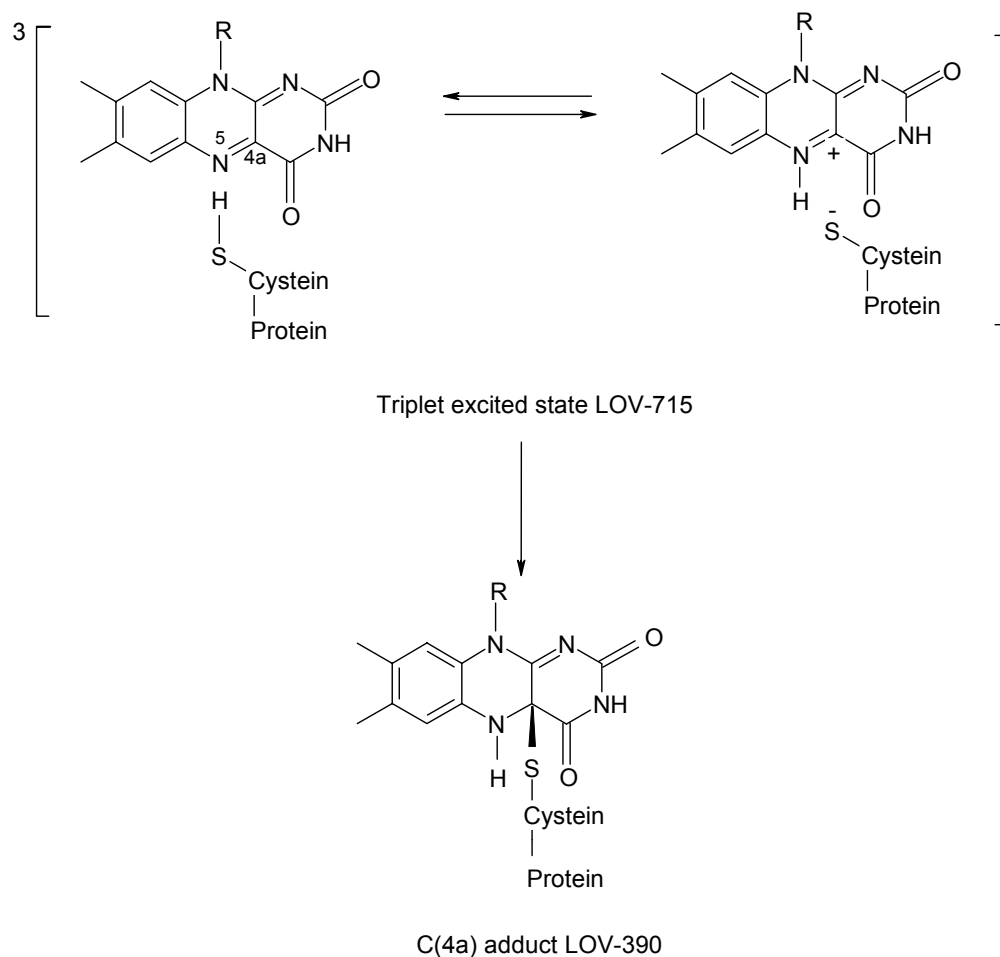


Figure 6.1. Ionic reaction scheme of the C(4a) adduct formation

6.1.2 Nucleophilic Model

The second hypothesis is a concerted mechanism proposed by Crosson and Moffat [42]. They considered that in LOV domains the close proximity of the cysteine side chain to C(4a) would favor nucleophilic attack of the cysteine thiolate anion on the isoalloxazine ring under certain

Mechanism of the formation of the adduct

conditions. The absorption of photons by the isoalloxazine ring causes a redistribution of electronic charges on the ring. In this theory, photoexcitation of FMN in LOV domains alters the electronic state of the isoalloxazine ring, and promotes base abstraction of the thiol proton by N(5), and nucleophilic attack of the thiolate anion on C(4a) to create the cysteinyl-flavin adduct (see Figure 6.2). Simply, the N(5) position of the FMN is protonated as the thiol sulfur attacks C(4a). The S-H proton moves toward the N(5) atom during the lifetime of the ^3FMN . Simultaneously, the extent of interaction between cysteine and C(4a) increases until the sulfur orbitals overlap with those of C(4a) and the photoadduct formation occurs.

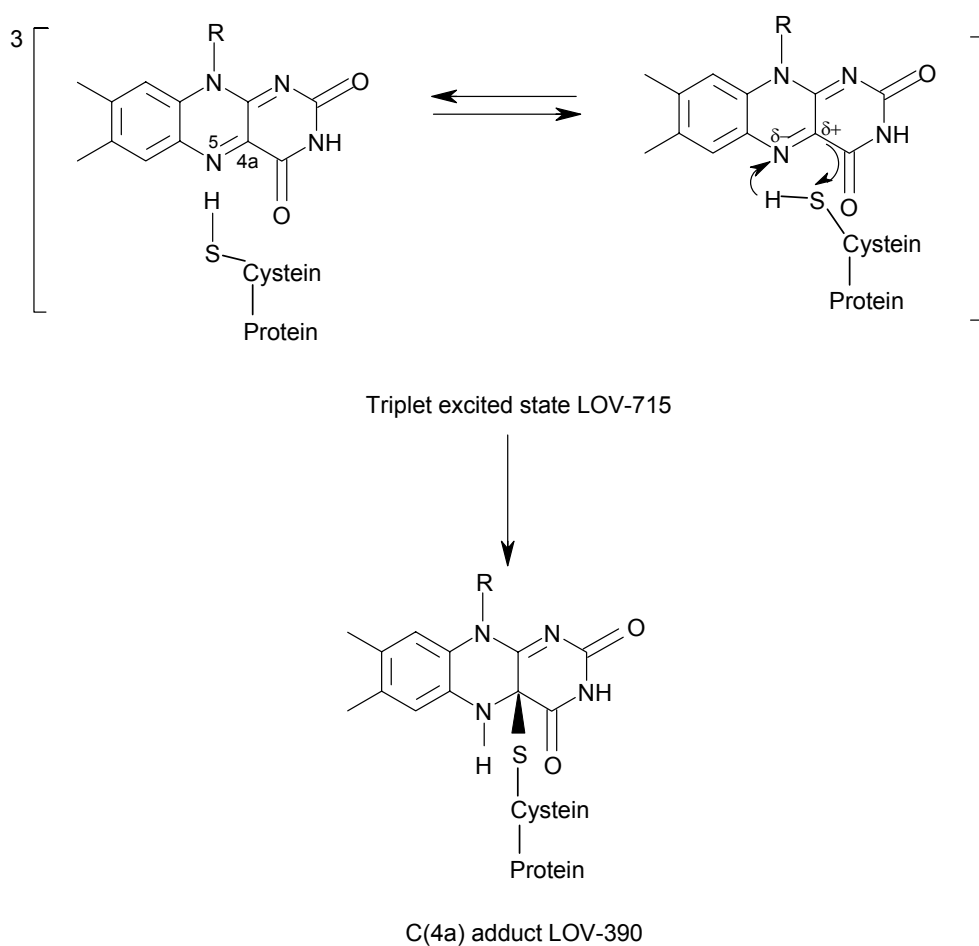


Figure 6.2. Concerted mechanism of the C(4a) adduct formation

6.1.3 Radical-pair Model

The third hypothesis is a neutral radical pair mechanism [33, 58]. ^3FMN is an efficient oxidizing agent in the presence of electron donors in solution, such as EDTA or Ethanthiol used in our experiment. A flavin semiquinone is formed from ^3FMN in a one-electron photoreduction that may be followed by photon transfer to give the neutral flavin radical during the suitable pH range (4.4 ~ 8.3). Then the radical pair forms the new compound through their recombination. Usually, the samples investigated in our measurements are all kept within this pH range. In our experiment with irradiation of LOV1-C57G mutant in the presence of ethanthiol, we observed the neutral flavin radical rather than an anion flavin radical. This is the expected first step in the radical mechanism. Hence we prefer the following neutral radical pair mechanism (see Figure 6.3): In the wild type, with a moderate light illumination, the chromophore FMN of the LOV domain dark form was excited into the triplet excited state, ^3FMN , which could abstract a hydrogen atom from the nearby residual, cysteine, and gives a neutral radical pair, FMNH^\cdot and RS^\cdot . Through the radical recombination, the neutral radical pair forms to the adduct LOV-390.

Although our experimental observation is consistent with this radical-pair reaction mechanism for adduct formation, the alternatives can still not be completely ruled out. On the other side, this mechanism is supported by increasing evidence from other experimental methods. Bittl and Kottke found a stable FMN-protein adduct that occurred upon illumination in LOV1-C57M mutant, which is quite compatible with the radical-pair mechanism [31, 32]. Neiss et al. calculated the electron distribution for a complex of isolumazine and methanethiol as a model for the FMN-thiol complex of LOV domains with *ab initio* methods. From an energetic point of view, adduct formation in the potential surface of the triplet state is impossible. They also

Mechanism of the formation of the adduct

favoured the radical mechanism [59]. More, Schleicher et al. believe it the most likely mechanism for explaining their observations obtained at low temperature [34]. So far, however, no radical-pair species could be observed with proper experimental means in photoexcited wild-type LOV domains.

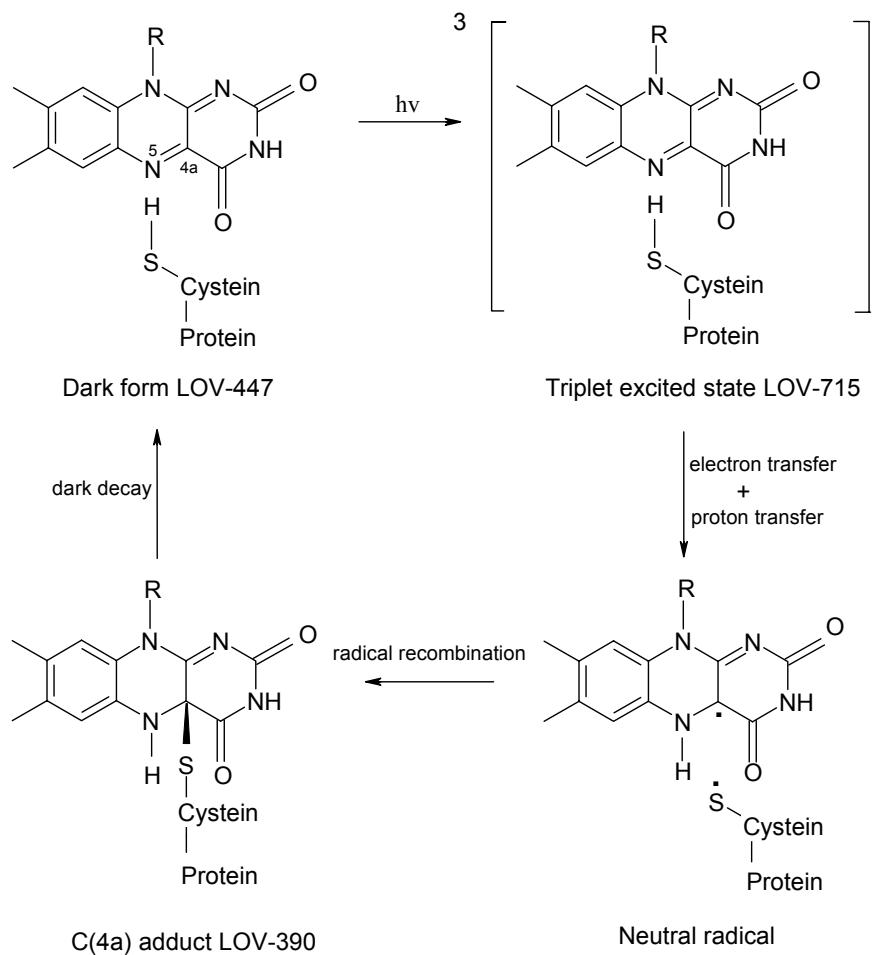


Figure 6.3. Radical reaction scheme of the C(4a) adduct formation

7 Summary

This dissertation investigated the photocycles of the two LOV domains from the phototropin Phot1 of *Clamydomonas reihadittii*. The main features of the photocycle of the LOV1 domain from this organism have been presented previously in the thesis of T. Kottke [39]. Here these investigations have been extended to the LOV2 domain and the construct containing both LOV domains, with emphasis on the mutual interaction of these domains and the influence of some external conditions like pH and salts.

All LOV domains contain the chromophore FMN which usually undergoes rapid and efficient electron transfer processes on light absorption [60-62]. It is now generally accepted, however, that the signaling state produced during the photocycles of the LOV domains in Phot proteins is the covalent adduct of a reactive cysteine with the FMN chromophore. This cysteine is Cys57 in LOV1 and Cys250 in LOV2. In addition to the photoactive domains LOV1, LOV2, and LOV1+2 the mutants LOV1-C57S, LOV2-C250S, LOV1+2-C57S, and LOV1+2-C250S have been studied. In these mutants the cysteine essential for the photoreaction is replaced by serine. Comparison with the absorption spectra in the dark reveals almost no differences between the various LOV domains. Only the mutants, in which the reactive cysteine was replaced by a nonreactive amino acid, show a slight blue-shift of the main absorption peak. In the double domains with single mutations in one domain, the spectra of the two domains cannot be

Summary

separated because of their complete overlap. Hence there is no evidence for any interaction between LOV1 and LOV2 domains in their dark states.

For both domains two intermediates in the photocycle could be identified. Based on the main absorption band at 715 nm and the sensitivity of the decay time on the presence of oxygen, the first intermediate (LOV-715) has been assigned to the triplet state of FMN. The second intermediate (LOV-390) is the Cystein-FMN adduct with a first absorption maximum at 390 nm.

In LOV2, the triplet state exhibits a monoexponential decay with a fast time constant (500 ns), whereas in LOV1, a biexponential decay is observed with 800 ns and 4 μ s [30]. The X-ray structure of LOV1 allowed to attribute this biexponential decay to the presence of two conformers in the dark state which differ in the relative orientation of the cysteine and the FMN. A similar X-ray structure is not available for the LOV2 domain, but the monoexponential decay of the triplet in this case suggests the presence of only one conformer. The monoexponential decay time of 500 ns for LOV2 is the shortest triplet lifetime reported so far for any LOV domain. This might be an indication for a very efficient formation of the adduct in this domain. In the mutants in which the essential cysteine is replaced by serine the triplet lifetime increases to 27 μ s for LOV1 and to 285 μ s for LOV2. This suggests the presence of a so far unidentified decay channel present in LOV1. The triplet kinetics in the double domains LOV1+2, LOV1+2-C57S, and LOV1+2-C20S are well described as the superposition of the decays of the single domains. Hence there is no evidence of an interaction between the domains on the level of their triplet states.

The decay kinetics of the adduct state of LOV2 appeared to be more complicated than that of LOV1, since a single exponential decay function was not adequate for the description for any condition of pH and salt concentrations. A phenomenological analysis in terms of a double

Summary

exponential decay could be applied, leading to the assignment of two species. Similar to the behaviour of LOV1 reported previously, the slower of these two decays is further slowed down by acidic conditions. This correlates with an increase observed for the activation energies of the thermal backreaction extracted from an Arrhenius analysis of the temperature dependence. In contrast to LOV1, an amplification of the pH effect by an increase of the ionic strength of the solution could not be observed for LOV2. A detailed analysis of this salt effect for LOV1 revealed that chloride ions have by far the strongest effect. The logarithmic dependence on concentration points, however, not to a well defined stoichiometry of the FMN-chloride interaction. Interestingly, this salt effect disappears when LOV1 is connected to an inactive LOV2-domain in LOV1+2-C250S. This might be explained by the assumption that the LOV2 covers the site at which chloride ions are adsorbed to LOV1.

A detailed analysis of the recovery kinetics of the dark states after adduct formation was undertaken based on a global fit to a sequence of kinetic traces observed for various excitation intensities and durations. The data for the single domains LOV1 and LOV2 could not be adequately fitted by models that include only three levels or consist of two non-connected two-level systems. A qualitatively acceptable fit was obtained only with a model that contained two dark states, two adduct states, and two intermediate states, with equilibrium between the ground states and the intermediates. The corresponding data for the two S-mutated double domains LOV1+2-C57S and LOV1+2-C250S, on the other hand, can be fitted with the three-level model (model II). This indicates an interaction between the two domains which blocks pathways of adduct decay that exist only in the isolated domains LOV1 and LOV2.

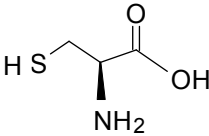
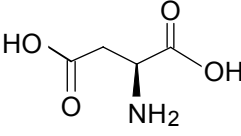
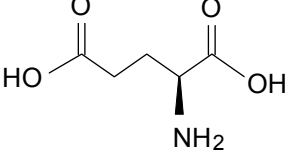
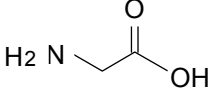
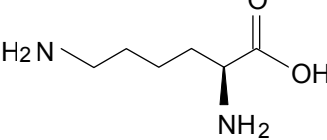
Our present state of knowledge on the photocycle of LOV2 is summarized in the scheme presented in Figure 4.1. The LOV2 dark form converts to the triplet state, LOV2-715, following excitation to the first excited singlet state. Then this triplet state leads to the long-lived

Summary

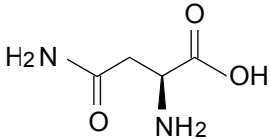
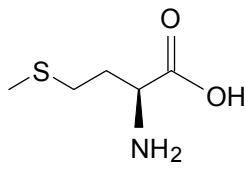
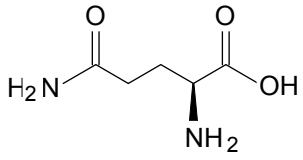
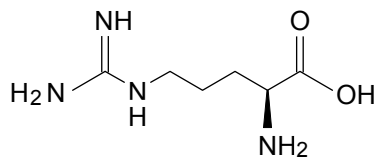
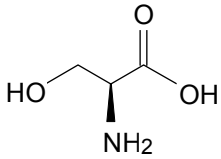
intermediate, LOV2-390, formation. The backreaction from LOV2-390 to LOV2-447 can be analyzed by a double exponential function under all external conditions studied, which means that there are two species involved in this process. However, they cannot be distinguished from their absorption spectra on their triplet level or in their dark forms.

8 Appendix

Structures of several amino acids mentioned in the dissertation:

Name	Abbr.	Structure
Cysteine	C	 <chem>NC(CS)C(=O)O</chem>
Aspartic acid	D	 <chem>NC(CC(=O)O)C(=O)O</chem>
Glutamic acid	E	 <chem>NC(CCC(=O)O)C(=O)O</chem>
Glycine	G	 <chem>NC(C=O)O</chem>
Lysine	K	 <chem>NC(CCN)C(=O)O</chem>

Appendix

Name	Abbr.	Structure
Asparagine	N	 <p>The structure shows a central carbon atom bonded to a hydrogen atom (not explicitly shown), an amino group (NH₂) pointing down, a carboxylic acid group (COOH) pointing up, and a side chain consisting of a methylene group (-CH₂-) attached to another carbon atom. This second carbon is bonded to a hydrogen atom (not explicitly shown), an amino group (NH₂) pointing down, and a carbonyl group (C=O) pointing up, which is further bonded to an amino group (H₂N).</p>
Methionine	M	 <p>The structure shows a central carbon atom bonded to a hydrogen atom (not explicitly shown), an amino group (NH₂) pointing down, a carboxylic acid group (COOH) pointing up, and a side chain consisting of a methylene group (-CH₂-) attached to another methylene group (-CH₂-), which is then attached to a sulfur atom (S).</p>
Glutamine	Q	 <p>The structure shows a central carbon atom bonded to a hydrogen atom (not explicitly shown), an amino group (NH₂) pointing down, a carboxylic acid group (COOH) pointing up, and a side chain consisting of two methylene groups (-CH₂-CH₂-) attached to a carbon atom. This carbon is bonded to a hydrogen atom (not explicitly shown), an amino group (NH₂) pointing down, and a carbonyl group (C=O) pointing up, which is further bonded to an amino group (H₂N).</p>
Arginine	R	 <p>The structure shows a central carbon atom bonded to a hydrogen atom (not explicitly shown), an amino group (NH₂) pointing down, a carboxylic acid group (COOH) pointing up, and a side chain consisting of three methylene groups (-CH₂-CH₂-CH₂-) attached to a nitrogen atom. This nitrogen is double-bonded to a carbon atom (C=NH) and single-bonded to a hydrogen atom (H) and an amino group (H₂N).</p>
Serine	S	 <p>The structure shows a central carbon atom bonded to a hydrogen atom (not explicitly shown), an amino group (NH₂) pointing down, a carboxylic acid group (COOH) pointing up, and a side chain consisting of a methylene group (-CH₂-) attached to a hydroxyl group (-OH).</p>

9 References

- [1] Short, T. W., Briggs, W. R. (1994) The transduction of blue light signals in higher plants. *Annu. Rev. Plant Physiol. Plant Mol. Biol.* 45, 143-171.
- [2] Briggs, W. R., Olney, M. A. (2001) Photoreceptors in plant photomorphogenesis to date. Five phytochromes, two cryptochromes, one phototropin, and one superchrome. *Plant Physiol.* 125, 85-88.
- [3] Briggs, W. R., Christie, J. M., and Salomon, M. (2001) Phototropins: A new family of flavin-binding blue light receptors in plants. *Antioxidants & Redox Signaling.* 3, 775-788.
- [4] Briggs, W. R., Huala, E. (1999) Blue-light photoreceptors in higher plants. *Annu. Rev. Cell Dev. Biol.*, 15. 33-62.
- [5] Batschauer, A., (1999) Light perception in higher plants. *Cell. Mol. Life Sci.* 55, 153-166.
- [6] Fankhauser C., Chory, J. (1999) Light receptor kinases in plants. *Curr. Biol.* 9, 123-126.
- Fedorov, R., Schlichting, I., Hartmann, E., Domratcheva, T., Fuhrmann, M., Hegemann, P. (2003) Crystal structures and molecular mechanism of a light-induced signaling switch: The Phot-LOV1 domain from *Chlamydomonas reinhardtii*. *Biophys. J.* 84, 2474-2482.
- [7] Cashmore, A. R., Jarillo, J. A., Wu, Y., Liu, D. (1999) Cryptochromes: blue light receptors for plants and animals. *Science* 284, 760-765.

References

- [8] Gomelsky, M and Klug, G (2002) BLUF: a novel FAD-binding domain involved in sensory transduction in microorganisms, *Trends Biochem. Sci.* 27, 497-500.
- [9] Laan, W., Bednarz, T., Heberle, J., Hellingwerf, K. J. (2004) Chromophore composition of a heterologously expressed BLUF-domain. *Photochemical & Photobiological Sciences* 3(11-12), 1011-1016.
- [10] Huala, E., Oeller, P. W., Liscum, E., Han, I. S., Larsen, E., Briggs, W. R. (1997) Arabidopsis NPH1: a protein kinase with a putative redox-sensing domain. *Science* 278, 2120-2123.
- [11] Van der Horst, M. A., and Hellingwerf, K. J. (2004) Photoreceptor proteins, “Star actors of modern times”: A review of the functional dynamics in the structure of representative members of six different photoreceptor families. *Acc Chem Res.* 37, 13-20.
- [12] Sprenger, W. W., Hoff, W. D., Armitage, J. P., and Hellingwerf, K. J. (1993) The eubacterium *Ectothiorhodospira halophila* is negatively phototactic, with a wavelength dependence that fits the absorption spectrum of the photoactive yellow protein, *J. Bacteriol.* 175, 3096-3104.
- [13] Spudich, J. L. (1998) Variations on a molecular switch: transport and sensory signalling by archaeal rhodopsins, *Mol. Microbiol.* 28, 1051-1058.
- [14] Iseki, M., Matsunaga, S., Murakami, A., Ohno, K., Shiga, K., Yoshida, K., Sugai, M., Takahashi, T., Hori, T., and Watanabe, M. (2002) A blue-light-activated adenylyl cyclase mediates photoavoidance in *Euglena gracilis*, *Nature* 415, 1047 – 1051.

References

- [15] Iino, M. (2001) Phototropism in higher plants. *In* D-P Häder, M Lebert, eds, Photomovement. *Elsevier Science*. 659–811.
- [16] Haupt, W. (1999) Chloroplast movement: from phenomenology to molecular biology. *Prog. Bot.* 60, 3-36.
- [17] Schroeder, J. I., Allen, G. J., Hugouvieux, V., Kwak, J. M., and Waner, D. (2001) Guard cell signal transduction. *Annu. Rev. Plant Physiol. Plant Mol. Biol.* 52, 627-658.
- [18] Briggs, W. R. and Christie J. M. (2002) Phototropin 1 and phototropin 2: Two versatile plant blue-light receptors. *Trends Plant Sci.* 7, 204–209.
- [19] Christie, J. M., Salomon, M., Nozue, K., Wada, M., Briggs, W.R. (1999) LOV (light, oxygen, or voltage) domains of the blue-light photoreceptor phototropin (nph1): Binding sites for the chromophore flavin mononucleotide. *Proc. Natl. Acad. Sci. USA* 96, 8779-8783.
- [20] Christie, J. M., Reymond, P., Powell, G. K., Bernasconi, P., Raibekas, A. A., Liscum, E., Briggs, W. R. (1998) *Arabidopsis* NPH1: A Flavoprotein with the properties of a photoreceptor for phototropism. *Science*, 282, 1698-1701.
- [21] Crosson, S., Rajagopal, S., and Moffat, K. (2003) The LOV domain family: photoresponsive signaling modules coupled to diverse output domains. *Biochemistry.* 42, 2-10.
- [22] Miller, S.M., Massey, V., Ballou, D., Williams, C. H., Jr., Distefano, M. D., Moore, M. J., Walsh, C, T. (1990) Use of a site-directed triple mutant to trap intermediates:

References

- demonstration that the flavin C(4a)-thiol adduct and reduced flavin are kinetically component intermediates in mercuric ion reductase. *Biochemistry* 39, 2831-2841.
- [23] Swartz, T. E., Corchnoy, S. B., Christie, J. M., Lewis, J. W., Szundi, I., Briggs, W. R., and Bogomolni, R. A. (2001) The photocycle of a flavin-binding domain of the blue light photoreceptor phototropin. *J. Biol. Chem.* 276, 36493-36500.
- [24] Salomon, M., Christie, J. M., Knieb, E., Lempert, U., Briggs, W. R. (2000) Photochemical and mutational analysis of the FMN-binding domains of the plant blue receptor, phototropin. *Biochemistry* 39, 9401-9410.
- [25] Salomon, M., Eisenreich, W., Dürr, H., Schleicher, E., Knieb, E., Massey, V., Rüdiger, W., Müller, F., Bacher, A., Richter, G. (2001) An optomechanical transducer in the blue light receptor phototropin from *Avena sativa*. *Biochemistry* 98, 12357-12361.
- [26] Swartz, T.E., Wenzel, P.J., Corchnoy, S.B., Briggs, W.R., Bogomolni, R.A. (2002) Vibration spectroscopy reveals light-induced chromophore and protein structural changes in the LOV2 domain of the plant blue-light receptor phototropin 1. *Biochemistry* 41, 7183-7189.
- [27] Crosson, S., and Moffat, K. (2002) Photoexcited structure of a plant photoreceptor domain reveals a light-driven molecular switch. *The Plant Cell* 14, 1067-1075.
- [28] Fedorov, R., Schlichting, I., Hartmann, E., Domratcheva, T., Fuhrmann, M., and Hegemann, P. (2003) Crystal structures and molecular mechanism of a light induced signaling switch: the Phot-LOV1 domain from *Chlamydomonas reinhardtii*. *Biophys. J.* 84, 2474-2482.

References

- [29] Kaiyao, H., Merkle, T., Beck, C.F. (2002) Isolation and characterization of a *Chlamydomonas* gene that encodes a putative blue-light photoreceptor of the phototropin family. *Physiol. Plant.* 115, 613-622.
- [30] Kottke, T., Heberle, J., Hehn, D., Dick, B., and Hegemann, P. (2003) Phot LOV1: Photocycle of a blue light receptor domain from the green alga *Chlamydomonas reinhardtii*. *Biophys. J.* 84, 1192-1201.
- [31] Bittl, R., Kay, C. W. M., Weber, S., Hegemann, P. (2003) Characterization of a flavin radical product in a C57M mutant of a LOV1 domain by electron paramagnetic resonance. *Biochemistry* 42, 8506-8512.
- [32] Kottke, T., Dick, B., Fedorov, R., Schlichting, I., Deutzmann, R., Hegemann, P. (2003) Irreversible photoreduction of flavin in a mutated Phot-LOV1 domain. *Biochemistry* 42, 9854-9862.
- [33] Kay, C. W. M., Schleicher, E., Kuppig, A., Hofner, H., Ruediger, W., Schleicher, M., Fischer, M., Bacher, A., Weber, S., Richter, G. (2003) Blue light perception in plants. *J. Biol. Chem.* 278, 10973-10982.
- [34] Schleicher, E., Kowalczyk, R.M., Kay, C.W.M., Hegemann, P., Bacher, A., Fischer, M., Bittl, R., Richter, G., Weber, S. (2004) On the reaction mechanism of adduct formation in LOV domains of the plant blue-light receptor phototropin. *J. A. Chem. Soc.* 126, 11067-11076.
- [35] Spudich, J.L., Yang, C.S., Jung, K.H., Spudich, E.N. (2000) Retinylidene proteins: structures and functions from archaea to humans. *Annu. Rev. Cell Dev. Biol.* 16, 365-392.

References

- [36] Harper, S. M., Neil, L.C., and Gardner, K. H. (2003) Structure basis of a phototropin light switch, *Science* 301, 1541-1544.
- [37] Kasahara, M., Swartz, T. E., Olney, M. A., Onodera, A., Mochizuki, N., Fukuzawa, H., Asamizu, E., Tabata, S., Kanegae, H., Takano, M., Christie, J. M., Nagatani, A., and Briggs, W. R. (2002). Photochemical properties of the flavin mononucleotide-binding domains of the Phototropins from Arabidopsis, rice, and *Chlamydomonas reinhardtii*. *Plant Physiol.* 129, 762-773.
- [38] Kagawa, T., Kasahara, M., Abe, T., Yoshida, S., and Wada, M. (2004) function analysis of phototropin2 using fern mutants deficient in blue light-induced chloroplast avoidance movement. *Plant Cell Physiol.* 45, 416-426.
- [39] Kottke, T. (2004) Spektroskopische Aufklärung des Photozyklus der LOV1-Domäne eines Phot-Blaulichtrezeptors.
- [40] Kanegae, H., Tahir, M., Savazzini, F., Yamamoto, K., Yano, M., Sasaki, T., Kanegae, T., Wada, M., Takano, M. (2000) Rice NPH1 homologues, OsNPH1a and OsNPH1b, are differently photoregulated. *Plant Cell Physiol* 41, 415-423.
- [41] Reymond, P., Short, T. W., Briggs, W. R. (1992) Blue light activates a specific protein kinase in higher plants, *Plant Physiol.* 100, 655-661.
- [42] Crosson, S., and Moffat, K. (2001) Structure of a flavin-binding plant photoreceptor domain: insights into light-mediated signal transduction. *Proc. Natl. Acad. Sci.* 98, 2995-3000.

References

- [43] Kennis, J. T. M., Crosson, S., van Gauden, M., Stokkum, Ivo H. M., Moffat, K., and van Grondelle, R. (2003) Primary reactions of the LOV2 domain of phototropin, a plant blue-light photoreceptor. *Biochemistry*. 42, 3385-3392.
- [44] Losi, A., Kottke, T., and Hegemann, P. (2004) Recording of blue light-induced energy and volume changes within the wild-type and mutated Phot-LOV1 domain from *Chlamydomonas reinhardtii*, *Biophys. J.* 86, 1051-1060.
- [45] Schüttrigkeit, T. A., C. K. Kompa, M. Salomon, W. Rüdiger, and M. E. Michel-Beyerle. 2003. Primary photophysics of the FMN binding LOV2 domain of the plant blue light receptor phototropin of *Avena sativa*. *Chem. Phys.* 294:501-508.
- [46] Holzer, W., Penzkofer, A., Susdorf, T., Alvarez, M., Islam, Sh. D. M., and Hegemann, P. (2004) Absorption and emission spectroscopic characterisation of the LOV2-domain of phot from *Chlamydomonas reinhardtii* fused to a maltose binding protein. *Chem. Phys.* 302, 105-118.
- [47] John B. Birks (1969) *Photophysics of Aromatic Molecules*, 492-513.
- [48] Fritz, B. J., Matsui, K., Kasai, S., and Yoshimura, A. (1987) Triplet lifetimes of some flavins. *Photochem. Photobiol.* 45, 539-541.
- [49] Corchnoy, S. B., Swartz, T. E., Lewis, J. W., Szundi, I., Briggs, W. R., and Bogomolni, R. A. (2003) Intramolecular proton transfers and structural changes during the photocycle of the LOV2 domain of Phototropin 1. *J. Biol. Chem.* 278, 724-731.
- [50] Kolbe, M., Besir, H., Essen, L. O., and Oesterhelt, D. (2000) Structure of the light-driven chloride pump halorhodopsin at 1.8 Å resolution. *Science* 288, 1390-1396.

References

- [51] Van Brederode, M. E., Hoff, W. D., Van Stokkum, I. H. M., Groot, M. L., and Hellingwerf, K. J. (1996) Protein folding thermodynamics applied to the photocycle of the photoactive yellow protein. *Biophys. J.* 71, 365-380.
- [52] Ataka, K., Heberle, J. (2004) Functional Vibrational Spectroscopy of a Cytochrome c Monolayer: SEIDAS Probes the Interaction with Different Surface-Modified Electrodes. *J. A. Chem. Soc.* 126, 9445-9457.
- [53] Gandour, R. D., and Schowen, R. L. (1978) *Transition States of Biochemical Processes.* 165-238.
- [54] Holzer, W., Penzkofer, A., Hegemann, P. (2005) Absorption and emission spectroscopic characterisation of the LOV2-His domain of phot from *Chlamydomonas reinhardtii*. *Chem. Phys.* 308, 79-91.
- [55] Handler, W., and Shrager, R. I. (1994) Deconvolutions based on singular value decomposition and the pseudoinverse: a guide for beginners. *J. Biochem. Biophys. Methods.* 28, 1-13.
- [56] Harper, S. M., Neil, L. C., Day, Iain J., Hore, P. J., and Gardner, K. H. (2004) Conformational changes in a photosensory LOV domain monitored by time-resolved NMR spectroscopy. *J. Am. Chem. Soc.* 126, 3390-3391.
- [57] Sakai, M., and Takahashi, H. (1996) One-electron photoreduction of flavin mononucleotide: time-resolved resonance Raman and absorption study. *J. Mol. Struct.* 379, 9-18.

References

- [58] Kay, C. W. M., Kuppig, A., Schleicher, E., Bacher, A., Richter, G., and Weber, S. (2002) Photochemistry of a C450A mutant of the LOV2 domain in Phototropin: Detection of a light-induced neutral flavin radical by EPR spectroscopy. In: *Flavins and Flavoproteins 2002*, Chapman, S., Perham, R., and Scrutton, N., Eds, Rudolf-Weber Agency for Scientific Publications, Berlin, 707-712.
- [59] Neiß, C., and Saalfrank, P. (2003) *Ab initio* quantum chemical investigation of the first steps of the photocycle of phototropin: a model study, *Photochem. Photobiol.* 77, 101-109.
- [60] Mataga, N., Chosrowjan, H., Shibata, Y., Tanaka, F., Nishina, Y., Shiga, K. (2000) Dynamics and Mechanisms of Ultrafast Fluorescence Quenching Reactions of Flavin Chromophores in Protein Nanospace. *J. Phys. Chem. B* 104, 10667-10677.
- [61] Zhong, D.P., Zewail, A.H. (2001) Femtosecond dynamics of flavoproteins: Charge separation and recombination in riboflavin (vitamin B2)-binding protein and in glucose oxidase enzyme. *Proc. Natl. Acad. Sci. USA.* 98, 11867-11872.
- [62] Aubert, C., Vos, M.H., Mathis, P., Eker, A.P.M., Brettel, K. (2000) Intraprotein radical transfer during photoactivation of DNA photolyase. *Nature* 405, 586-590.

Acknowledgement

Firstly, I would thank Prof. Dr. B. Dick for his offering this precious opportunity to me, coming to this beautiful country and proceeding my study. In my work, he gave me many helps and good advices. During the period of writing my thesis, his encouragement made me finishing it smoothly. Here I express my deep appreciation to him! Also, I would like to thank Prof. Dr. P. Hegemann. He had also given me many helpful discussions and advices. Thank him very much!

Specially thank Dr. Tilman Kottke, he gave me many helpful discussion and inspiration in my experiment. Here I express my gratitude for his kindness and helps.

I thank Tina Schiereis for her excellent technical assistance.

My colleagues, Walter Finkenzeller, Dr. Cornelius Kratzer, Dr. Rudolf Lehnig, Dr. Jinnan Liu, Dr. Thorsten Oberhuber, and Tanja Schaffer, offered me many helps in my work and made many funs during lunch-time. I express my appreciation to them for their kindness.

I would also like to thank the many people who have given me many helps in my work, Frau Alder, Frau Berg, Frau Höing and Frau Müller for their kind assistance.

My family and my friends always support me. Here I express my sincere gratitude to them.

At last, I pay my grateful acknowledgement for DFG (Deutsche Forschungsgemeinschaft) offering me the stipends in last three years.